

**THE CREATION OF LOW
ACTIVITY MÖSSBAUER SOURCES
FOR UNDERGRADUATE
RESEARCH**

By

August Gula

A thesis submitted in partial fulfillment of the
requirements for the degree of

Bachelor of Science

Houghton College

May 2016

Signature of Author.....

Department of Physics
May 5, 2016

.....

Dr. Mark Yuly
Professor of Physics
Research Supervisor

.....

Dr. Kurt Aikens
Assistant Professor of Physics

**THE CREATION OF LOW
ACTIVITY MÖSSBAUER
SOURCES FOR
UNDERGRADUATE
RESEARCH**

By

August Gula

Submitted to the Department of Physics
on May 5, 2016 in partial fulfillment of the
requirement for the degree of
Bachelor of Science

Abstract

An experimental test of general relativity can be made using the transverse Doppler effect. The design of the experiment conducted at Houghton College has entailed the development of low activity Mössbauer sources. These low activity sources are made out of small amounts (less than 1 μCi) of ^{57}Co that are electroplated onto thin steel foils (0.0254 mm) and heated to 1000°C in a vacuum. The use of these weak sources should be possible with coincidence techniques to reduce the background rate. A rotating disk absorber will be used for longitudinal Doppler effect tests prior to developing the transverse Doppler effect apparatus. A procedure for creating low activity Mössbauer sources has been developed, including three methods to measure the source activity, and an experimental apparatus for demonstrating the longitudinal Doppler effect.

Thesis Supervisor: Dr. Mark Yuly

Title: Professor of Physics

TABLE OF CONTENTS

Chapter 1 History	6
1.1 Discovery.....	6
1.2 Connection to General Relativity	8
1.3 Additional General Relativity Experiments.....	11
1.3.1 H.J. Hay and T.E. Cranshaw Experiment (1960).....	12
1.3.2 The Kündig Experiment (1962).....	14
1.3.3 The Kholmetskii Experiment (1996)	16
1.4 The Mössbauer Effect at Houghton College	19
Chapter 2 Theory	24
2.1 Nuclear Resonance Fluorescence.....	24
2.1.1 Recoil vs. Recoilless Emission.....	25
2.1.2 Conservation of Energy.....	26
2.1.3 Mean Line Width	26
2.1.4 Doppler Broadening.....	28
2.2 What Makes a Good Absorber?	29
2.3 Calculating the Rotation Speed for the Absorber	31
2.4 The Transverse Doppler Effect	34
2.5 Gravitational Redshift	36
Chapter 3 Experiment.....	38
3.1 Making a Mössbauer Source.....	38
3.1.1 Contamination Prevention.....	38
3.1.2 Removing Particulates and Organics Materials.....	39
3.1.3 Removing Inorganic Materials	39
3.1.4 Mixing the Radioactive Solution	39
3.1.5 Electroplating.....	40
3.1.6 Diffusion of ⁵⁷ Co.....	42
3.2 Vacuum System.....	44
3.3 Methods of Measuring the Source Activity	44
3.3.1 Method 1: Change in Mass.....	45
3.3.2 Method 2: Electroplated Charge	46
3.3.3 Method 3: Radioactivity.....	50

3.4 Longitudinal Doppler Effect Apparatus	55
Chapter 4 Conclusion and Future Plans	59
Appendix Experimental Procedure.....	60

TABLE OF FIGURES

Figure 1. Example of Resonance Fluorescence.....	6
Figure 2. Recoilless Emission vs. Recoil Emission.....	8
Figure 3. Recoil vs. Recoilless Breit-Wigner Distributions.....	9
Figure 4. Hay and Cranshaw Apparatus.....	13
Figure 5. Hay and Cranshaw Experimental Results.....	14
Figure 6. Kündig Apparatus.....	16
Figure 7. Kündig Experimental Results.....	17
Figure 8. Theory Compared with Kündig Results.....	18
Figure 9. Kholmetskii et al. Apparatus.....	19
Figure 10. Kholmetskii et al. $K_4Fe(CN)_6 \cdot 3H_2O$ Absorber Results.....	20
Figure 11. Kholmetskii et al. $Li_3Fe_2(PO_4)_3$ Absorber Results.....	20
Figure 12. The Decay Scheme of ^{57}Co	22
Figure 13. Longitudinal Doppler Effect Apparatus.....	23
Figure 14. Transverse Doppler Effect Apparatus.....	23
Figure 15. Atomic Resonance Fluorescence.....	24
Figure 16. Overlap of the Breit-Wigner Distributions.....	30
Figure 17. Relativistic Effects on Light.....	31
Figure 18. Electroplating Apparatus.....	41
Figure 19. Electroplating Circuit Diagram.....	42
Figure 20. Electroplating Current Vs. Time Data.....	43
Figure 21. Furnace Apparatus.....	45
Figure 22. Temperature Vs. Current Measurements.....	47
Figure 23. Cobalt Diffusion Apparatus.....	48
Figure 24. Resistivity Measurements.....	48
Figure 25. Diagram of the Aluminum Shield System.....	49
Figure 26. Radioactive Counting Apparatus.....	53
Figure 27. Histogram for the Source Bottle of ^{57}Co	54
Figure 28. Background Radioactivity Histogram.....	54
Figure 29. Copper Rods Radioactivity Histogram.....	55
Figure 30. Vacuum Chamber Radioactivity Histogram.....	56
Figure 31. Radioactivity Histogram of Waste Solution.....	56
Figure 32. Longitudinal Doppler Effect Apparatus.....	57
Figure 33. Longitudinal Doppler Effect Circuit Diagram.....	58

1.1 Discovery

At the turn of the 20th century, Lord Rayleigh suggested [1] the existence of atomic resonance fluorescence, the absorption and reemission of characteristic photons due to atomic excitation states, and suggested an attempt should be made to observe resonance fluorescence experimentally. Resonance fluorescence is the process in which the de-excitation photons of an atom are reabsorbed by a neighboring atom with the same atomic structure, shown in Figure 1. In 1904 R.W. Wood conducted an experiment [2] that demonstrated this process. Using sodium vapor he demonstrated the absorption and reemission of the two D-lines of sodium, which differ only by a few tenths of a nanometer in wavelength. However, it was assumed in these experiments that the absorption resonance was exactly the same frequency as the emitted radiation.

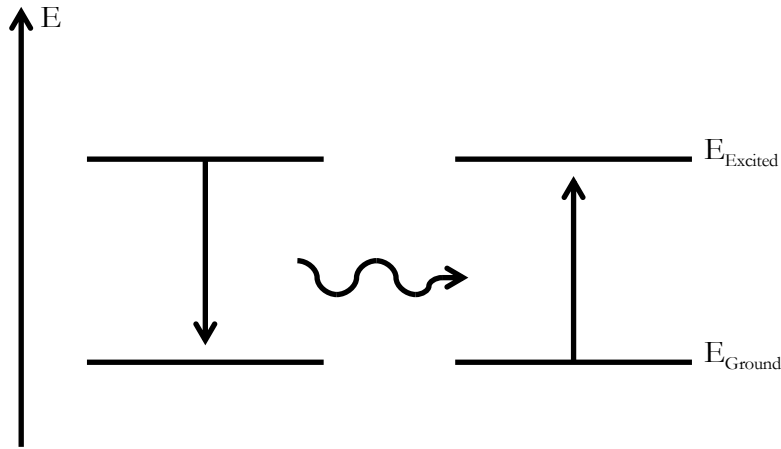


Figure 1. Example of resonance fluorescence. An atom in an excited state returns to the ground state by the emission of a photon. That emitted photon can then be subsequently reabsorbed by a neighboring identical atom. This process was demonstrated by R.W. Wood in 1904.

It was then suggested by W. Kuhn in 1929 that nuclear resonance could also be observed [3]. That is, the emission of characteristic photons and the subsequent reabsorption by a nucleus of the same isotope. This process is analogous to that illustrated in Figure 1. As an example of nuclear resonance fluorescence, a ^{57m}Fe nucleus could emit a gamma ray that could be reabsorbed by another ^{57}Fe nucleus. However, to the surprise of many physicists at the time, this physical process was not experimentally found.

In 1938 W. Lamb wrote an article [4] on the capture of neutrons in a crystal lattice. In it, he predicted the shift of resonance peaks due to the recoil of the nucleus. These resonance peaks are Breit-Wigner distributions, also called Lorentzian distributions, and will be explained in more depth in Section 2.1.3. A Breit-Wigner distribution describes the probability distribution of a nuclear emission as a function of energy. By taking inspiration from W. Lamb's work, Mössbauer used this theory to explain the results he found in 1958.

In 1958 R. Mössbauer performed an experiment [5] using a cold ^{191}Os source in which nuclear resonance fluorescence was observed. The parent nucleus, ^{191}Os decays by electron emission, leaving a daughter ^{191}Ir nucleus. When he cooled the apparatus down, he observed the nuclear resonance fluorescence of ^{191}Ir . This is because the now cooled emitter and absorber were both members of a rigid crystal lattice. He demonstrated that nuclear resonance was not previously observed because the emitting atom recoils upon the release of a gamma ray, and the gamma ray causes the absorbing nucleus to recoil also.

This recoil reduced the gamma ray energy as a result of the conservation of linear momentum. Because the emitting nucleus recoils, it carries away some of the energy released in the decay, reducing the energy available for the photon. Similarly, when the absorbing nucleus recoils, some the energy of the photon goes into the kinetic energy of the recoiling nucleus, leaving less available for exciting the nucleus, as shown in Figure 2. This loss of energy was the key reason why nuclear resonant fluorescence and absorption was not observed. Because these Breit-Wigner distributions are so

narrow, if the energy lost due to recoil is much greater than the line width of the distribution, that is the full width half maximum (FWHM) of the distribution, then the overlap of the emission of absorption lines approaches zero. Figure 3 shows a basic example of the concept of recoilless emission versus recoiled emission.

The Mössbauer effect is the reduced nuclear recoil due to the momentum transfer to the rigid lattice of a crystal structure rather than a single free nucleus. This reduces the shift in the resonant absorption and emission peaks, as shown in Figure 3. In 1961 R. Mössbauer was awarded the Physics Nobel Prize for his research and discovery [3].

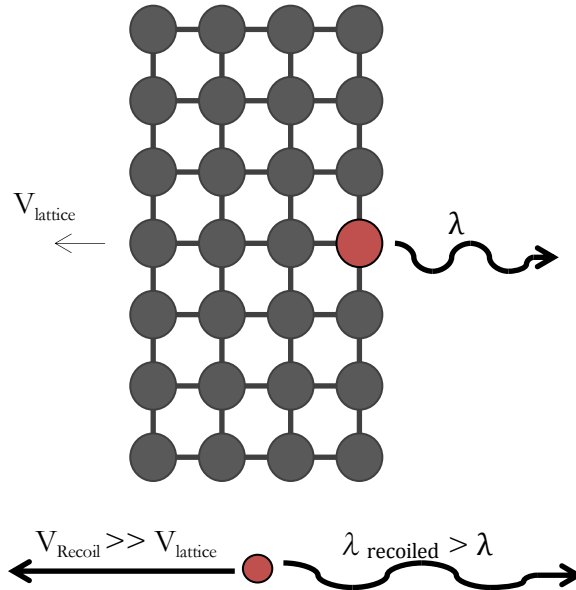


Figure 2. Recoilless emission vs. recoil emission. The large lattice recoils with very little velocity compared to the recoil emission. Since this is the case, the kinetic energy transferred into the parent nucleus is far less than if the nucleus were free. The free nucleus recoils with a velocity magnitude greater than that of the recoilless case. Thus, kinetic energy was taken away from the gamma ray by the nucleus, which causes the emitted gamma ray to be red-shifted.

1.2 Connection to General Relativity

Mössbauer's finding was rapidly employed in nuclear science, chemistry, and to test general relativity. The use of the Mössbauer effect allows for the very precise measurement of frequencies, to one part in

about 10^{15} . In order to use the Mössbauer effect, a radioactive parent is embedded into a crystal lattice and the absorbing daughter nuclei into another crystal lattice such that the recoil energy loss is reduced for both nuclei. A second way to overcome nuclear recoil is by giving the parent or daughter nucleus a component of velocity in the direction of the other. That is, in essence, to use the longitudinal Doppler effect to shift the frequency to increase the overlap of the emission and absorption distributions. In demonstrating general relativity, rather than the longitudinal Doppler shift, the gravitational redshift or blueshift, caused by the transverse Doppler effect, is used.

Gravitational redshift (or blueshift) is the shift in the wavelength of a photon due to the loss (or gain) of energy of a photon changing position in a gravitational potential. This effect demonstrates Einstein's theory of general relativity in that massless particles such as photons are affected by the curvature of spacetime around massive objects. This effect has been used, in combination with the Mössbauer effect, to demonstrate general relativity experimentally.

Soon after the discovery of the Mössbauer effect using cold ^{191}Ir , it was discovered that the Mössbauer effect allowed nuclear resonance fluorescence in ^{57}Fe at room temperature [7]. At Harvard University R. V. Pound and G. A. Rebka Jr employed ^{57}Fe resonance fluorescence in experiments to demonstrate general relativity [8-11]. The ^{57}Fe isotope was especially suitable because of its narrow line width of 10^{-8} eV, which is small compared to the recoil energy of 0.002 eV. Because of this attribute, ^{57}Fe proved to be useful in measuring the gravitational redshift. Pound and Rebka used a polished beryllium disk electroplated with enriched iron. The electroplated absorption target used 80 mg of iron, 31.79% of which was ^{57}Fe . A ^{57}Co source was created at Oak Ridge National Laboratory by electroplating ^{57}Co onto one side of a steel foil. The source was then diffused into the lattice at temperatures of 900-1000 °C for one hour [10]. The source used was 400 mCi.

In the experiment there were two setups, one in which the source was placed at the top of a 22.56 meter tower and the absorber was placed at the bottom, the other with the positions of the source and the absorber reversed. In both cases, a cylindrical 3 in. \times 1/4 in. NaI detector was placed near the

source to determine how many counts to expect at the absorber as well as to monitor the activity of the source.

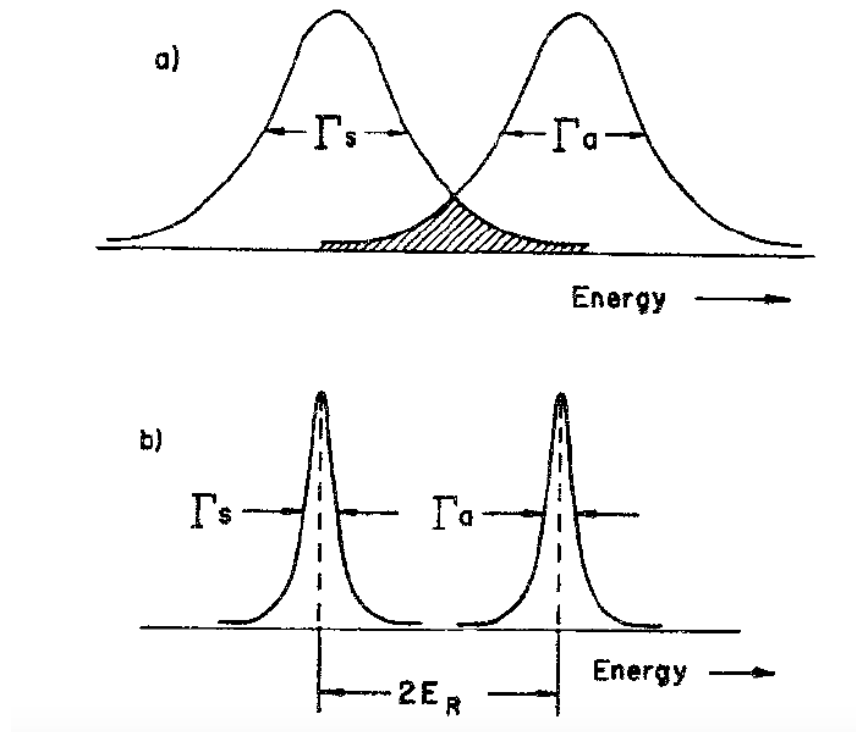


Figure 3. Recoil vs. recoilless Breit-Wigner distributions. In (a) the Mössbauer effect reduced the recoil of the source (s) such that the Breit-Wigner distribution of the emission overlaps with the absorption distribution, which allows the nuclear resonance fluorescence to occur. Γ_s and Γ_a are the FWHM of the Breit-Wigner distributions for the source and the absorber, respectively. In (b) recoil is present and causes the peaks to be shifted apart by twice the recoil energy E_R , such that the Breit-Wigner distributions no longer overlap and nuclear resonance fluorescence does not occur. Figure taken from Ref. [6].

The ^{57}Co source was connected to a transducer, which oscillated the source back and forth sinusoidally with a maximum speed of 0.01 cm/sec to use the longitudinal Doppler shift to observe the gravitational redshift. This allowed the experiment to sweep the spectrum of relative frequency shifts

of the emitter. The data received during each quarter cycle of the oscillation of the transducer was sorted based on the velocity of the transducer and whether it was moving toward or away from the absorber.

In between the source and the absorber was a cylindrical mylar bag which was filled with helium flowing at a rate of 30 liters/hr. This swept out air diffusing into the bag to reduce the attenuation of the gamma rays. It was also necessary to ensure that the source and absorber were at the same temperature, since a difference of even 0.6 °C was enough to produce a Doppler broadening that would cause a frequency shift as large as that sought to be observed [10].

The frequency shift was determined by taking multiple counting runs over several days and then switching the source/absorber orientation and averaging over different runs with corrections for the temperature differences between the source and absorber. The frequency shifts were small compared to the emitted frequency, on the order of 10^{-15} of the total frequency. Making these corrections they measured the gravitational redshift to be within 5% of theory predictions. Their results are displayed in Table 1 [10]. Because these shifts are so incredibly small, the ability to use the Mössbauer effect was essential.

What the Pound and Rebka observed was extraordinary. They measured the fraction of Doppler shift due to the gravitational redshift of a few meters difference in elevation on earth, and their experiment was one of the strongest early confirmations of Einstein's general theory of relativity.

1.3 Additional General Relativity Experiments

After the discovery of the Mössbauer effect, several other experiments, in addition to the Pound and Rebka experiment used the Mössbauer effect to test general relativity [12-14]. As previously mentioned, this is possible because of the small (10^{-15}) fractional shifts in the frequency that can be measured using the Mössbauer effect. These other experiments placed the absorber on a rotating frame in which it experienced a constant centripetal acceleration, which, using the equivalence principle is equivalent to a gravity field. Hence one would expect a gravitational redshift. By doing this,

researchers could test general relativity based on using the transverse Doppler effect observed between the emitted gamma ray and the absorber in an accelerated reference frame.

Table 1. Pound and Rebka's observed experimental results. Gravitational redshift was shown in this experiment by the observed frequency shifts of the gamma ray propagating between the top of the experimental apparatus to the bottom. The values of these shifts are recorded in the table as fractional frequency (10^{-15}) differences. The fractional shift was determined using the velocity of the transducer while nuclear resonance fluorescence was being observed. The temperature correction was calculated by determining the temperature difference between the source and the absorber. The net shift is the algebraic sum of the shift observed and the temperature correction. This table was taken from Ref. [9].

Period	Shift observed	Temperature correction	Net shift
Source at bottom			
Feb. 22, 5 p. m.	-11.5 ± 3.0	-9.2	-20.7 ± 3.0
	-16.4 ± 2.2 ^a	-5.9	-22.3 ± 2.2
	-13.8 ± 1.3	-5.3	-19.1 ± 1.3
	-11.9 ± 2.1 ^a	-8.0	-19.9 ± 2.1
	-8.7 ± 2.0 ^a	-10.5	-19.2 ± 2.0
Feb. 23, 10 p. m.	-10.5 ± 2.0	-10.6	-21.0 ± 2.0
	Weighted average = -19.7 ± 0.8		
Source at top			
Feb. 24, 0 a. m.	-12.0 ± 4.1	-8.6	-20.6 ± 4.1
	-5.7 ± 1.4	-9.6	-15.3 ± 1.4
	-7.4 ± 2.1 ^a	-7.4	-14.8 ± 2.1
	-6.5 ± 2.1 ^a	-5.8	-12.3 ± 2.1
	-13.9 ± 3.1 ^a	-7.5	-21.4 ± 3.1
Feb. 25, 6 p. m.	-6.6 ± 3.0	-5.7	-12.3 ± 3.0
	-6.5 ± 2.0 ^a	-8.9	-15.4 ± 2.0
	-10.0 ± 2.6	-7.9	-17.9 ± 2.6
Weighted average = -15.5 ± 0.8			
Mean shift = -17.6 ± 0.6			
Difference of averages = -4.2 ± 1.1			

^aThese data were taken simultaneously with a sensitivity calibration.

1.3.1 H.J. Hay and T.E. Cranshaw Experiment (1960)

Soon after Mössbauer made his discovery, H.J. Hay and T.E. Cranshaw at the Atomic Energy Research Establishment in the United Kingdom conducted an accelerating absorber experiment [13]. Applying the equivalence principle they attempted to measure the gravitational redshift of the gamma

rays using an absorber on the radius of a spinning system. In order to do this, a source was placed at the center of a rotating frame with an absorber at a given radius.

As shown in Figure 4, a ^{57}Co source was electroplated on the surface of a 0.08 mm-diameter iron cylinder. The cylinder was then mounted between two plates. In between the plates a highly enriched, 50% ^{57}Fe foil, of thickness 3.5 mg cm^{-2} , was placed on the inside of a lucite cylindrical shell, of diameter 13.28 cm. This lucite cylindrical shell was of large enough diameter that the absorber was near the edge of the plates.

A xenon-filled proportional counter was placed near the rotating source and absorber assembly, behind lead bricks with a thin slit for the unabsorbed gamma rays to pass through. This detector was used to determine the ratio of counts referenced to the motionless state, because the absolute radioactivity of the source was unknown.

The results from their experiment, shown in Figure 5, agree with the theory expectations. However, their results suffered from several problems, such as the unknown radioactivity of the ^{57}Co source. Also, this experiment created a source distribution that acted as a line distribution source, which could

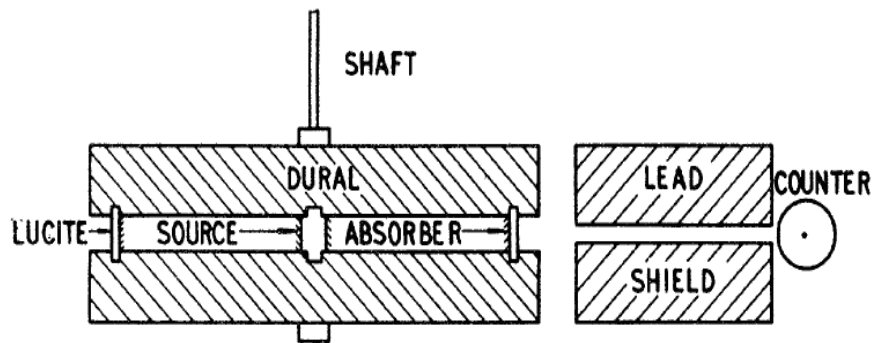


Figure 4. Hay and Cranshaw's apparatus. The ^{57}Co source was placed on the central axis and was spun with the shaft. The lucite cylindrical shell had a 50% ^{57}Fe enriched iron foil glued to the inside face. This foil acted as the absorber for the gamma rays, which were detected. Figure taken from Ref. [13].

have caused complications that may not have been properly accounted for in the analysis of the experiment.

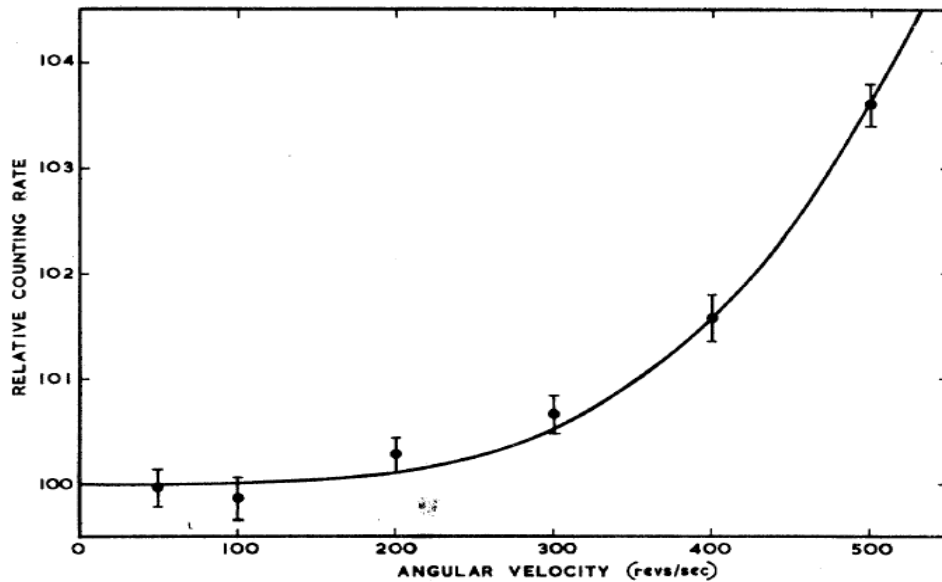


Figure 5. Hay and Cranshaw experimental results. The theory curve agreed well with Hay and Cranshaw's data points. Figure taken from Ref. [13].

1.3.2 The Kündig Experiment (1962)

W. Kündig performed a similar experiment [12] to test general relativity through the transverse Doppler effect with an accelerating absorber. A ^{57}Co source was placed at the center of an ultracentrifuge with the absorber target at a given radius from the center. A diagram is shown in Figure 6. By placing the absorber, an ^{57}Fe enriched foil, on the radius of the centrifuge rotor, the frame of the absorber experienced the equivalent to a gravitational redshift through the equivalence principle of general relativity.

The cylindrical central rotor was machined of a special alloy of aluminum with a diameter of 20 cm. The absorber source foil was 91% enriched ^{57}Fe , and was mounted to a thin thick acrylic disk placed at

a radius of 9.3 cm from the center. The ^{57}Co source was 10 mCi electroplated onto a 3 mm \times 8 mm iron foil. The iron foil and acrylic mount were then glued on the face of a piezoelectric transducer, and were placed at the center of the centrifuge. The piezoelectric transducer allowed the source's velocity to change relative to the absorber. This enabled observation of the entire resonance line at various values of rotational speed. The speed of the rotor was regulated manually, with an error up to 0.1%. The chamber containing the rotor was evacuated to avoid frictional heating. On the outside of the rotor chamber there were two proportional counters, each on opposite sides of the apparatus. The rotational speed of the centrifuge was 50 rev/sec to 500 rev/sec.

Krypton filled proportional counters, similarly to the Hay and Cranshaw experiment, measured the fraction of transmitted gamma rays as a function of the speed of the spinning rotor and transducer velocity. These measurements were recorded and sorted based on the radial velocity of the source.

By using the transducer to move the source longitudinally, the experiment was able to measure the small frequency shifts due to the acceleration. A plot of the counting rate versus the absorber velocity is given in Figure 7. The results are shown in Figure 8.

Predictions from general relativity agreed within 1.1% with the results of the experiment, which was an astounding result for the time, and even today. However, in 1996, A.L. Kolmetskii et al. re-analyzed Kündig's results and found that there was error related to a coefficient in the expansion that was used. The coefficient of $\frac{1}{2}$, from the binomial expansion of the transverse Doppler effect, seemed wrong. As a result Kolmetskii conducted a new experiment to test the higher order terms of the transverse Doppler effect, that is, orders of $\left(\frac{v^2}{c^2}\right)$ and higher [10,13] as in Eq. 1.3.1. In the transverse Doppler effect the energy of a gamma ray can be found as a function of the absorber's velocity,

$$E' \cong E \left(1 - \frac{1}{2} \left(\frac{v}{c} \right)^2 + \dots \right) \quad (1.3.1)$$

where E' is the energy observed in a frame with velocity v , and E is the energy of the gamma ray when it was emitted.

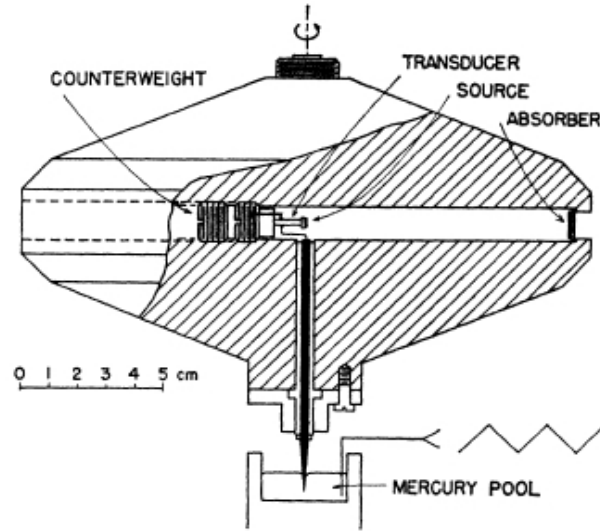


Figure 6. Kündig apparatus. The principle of this experiment was to use the acceleration difference in the reference frames of the source located at the center of the centrifuge and the absorber located on the far edge to cause an apparent red-shift of the incoming gamma ray in the frame of the absorber. Figure taken from Ref. [12].

1.3.3 The Kholmetskii Experiment (1996)

Kholmetskii et al. [14] discovered that Kündig's analysis of his experimental data was incorrect; a miscalculation of the coefficient on the second order Doppler shift term was found. This coefficient value, k , predicted by general relativity (see Eq. 1.3.1 or Sections 2.4 or 2.5) is $1/2$. However, reanalyzing the data of Kündig, it was found that $k = 0.596 \pm 0.006$ is a better fit. It was suggested by Kholmetskii et al. that this could be due to the vibration of the apparatus itself. Kündig considered these vibrations and did much work to prevent them, due to this he believed that they were a source of very little systematic error. These vibrations cause a line broadening of the resonance peaks. Because of the discrepancy between Kündig's recalculated experimental results and the value predicted by theory, the need for another experiment became apparent.

As shown in Figure 9, an experiment similar to Kündig's, using an ultracentrifuge was performed [15]. The rotor system was based on the K-80 ultracentrifuge with a diameter of 630 mm, having a range of rotational frequencies of 0-150 rev. sec⁻¹. This rotor system could reach maximum speeds far greater than Kündig's experiment.

The ^{57}Co source was in a $^{57}\text{Co}(\text{Cr})$ alloy with an activity of 20 mCi; this alloy was a face-centered cubic atomic structure. The source was placed into a Cu-Pb shield and collimating system, which was mounted on the rotation axis. A semi-hermetic chamber was used and pumped down to 100 Torr during measurements. The temperature of the source and the absorber was not allowed above 10 °C, regardless of the presence of rotor heating due to frictional effects.

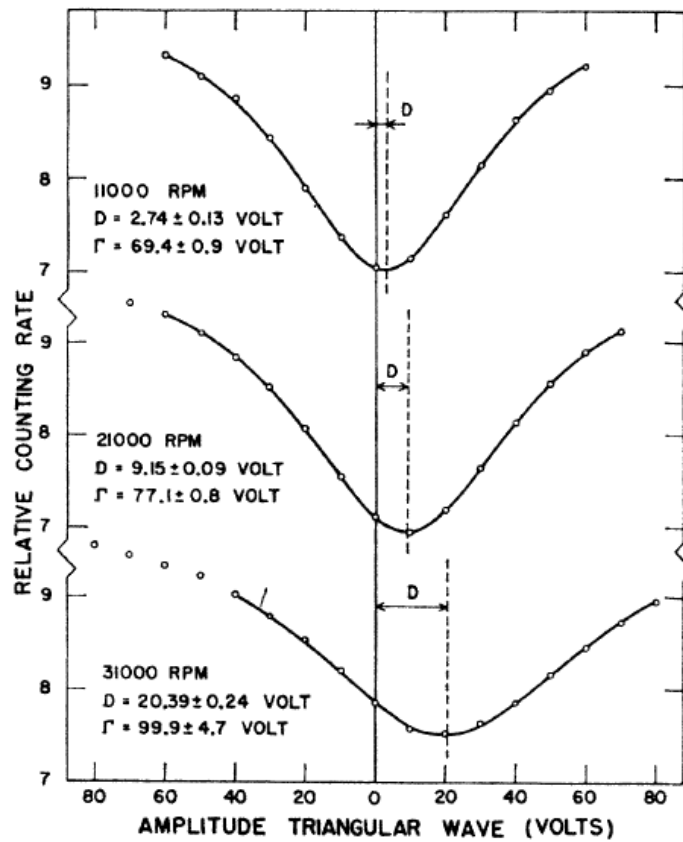


Figure 7. Kündig's experimental results. The three different curves are three different rotor speeds. The curves are normalized such that at if the voltage were infinite, the relative count rate would be 10. The variable D is the velocity of the transducer recorded in volts, and corresponds to the shift in absorption peak. The FWHM of the resonance peak is Γ . Figure taken from Ref. [12].

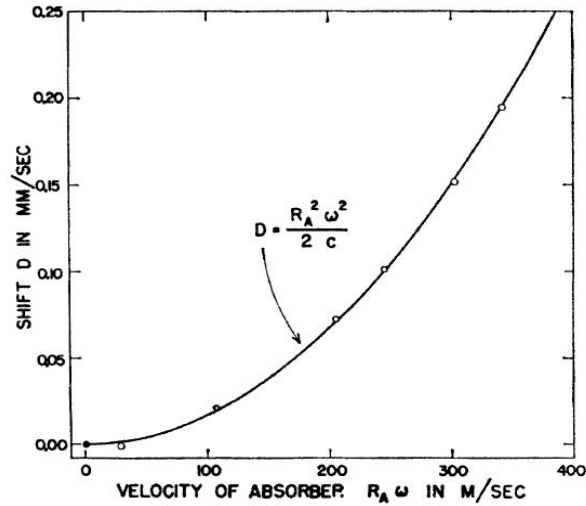


Figure 8. Theory compared with Kündig results. Kündig's experiment had excellent correlation. This theory agrees with the experimental data points to 1.1%. Figure taken from Ref. [12].

A xenon-filled proportional counter was placed behind collimating shielding. Two different types of 15 mm \times 55 mm absorber plates were used. The first absorber was $K_4Fe(CN)_6 \cdot 3H_2O$ enriched to 90% ^{57}Fe . The second absorber was made of $Li_3Fe_2(PO_4)_3$ enriched with 90% ^{57}Fe .

The results of the Kholmetskii experiment are shown in Figures 10 and 11. Kholmetskii reported [14] that they chose to “... neglect the variation of the resonant line position due to thermal shift.” Whereas Pound and Rebka report [10] that the difference of even 0.6 °C was enough to cause a shift equal to the frequency shift that is to be observed. Kholmetskii allowed for up to 10 °C difference between the source and absorber. It could be the case that the resonance shift sought by Kholmetskii was far greater than that of the Pound and Rebka experiment, and thus would have had greater tolerance for thermal shift. However, whether this assumption may have caused the variation in Kholmetskii's data from theory predictions should be examined.

The fit of the Kholmetskii et al. data yielded the coefficient, k , on the second order term of Eq. 1.3.1,

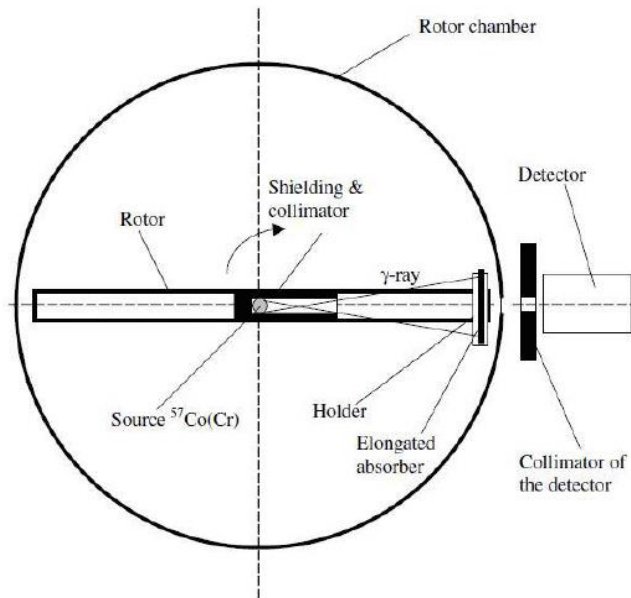


Figure 9. Kholmetskii et al. apparatus. The $^{57}\text{Co}(\text{Cr})$ source was placed on the central rotation axis of the rotor and inside a Cu-Pb collimating shield. The 14.4 keV gamma rays were collimated toward the 15 mm \times 55 mm absorber foil. The xenon-filled proportional counter was used to determine the number of counts relative to the stationary state of the apparatus before the rotor was activated. Figure taken from Ref. [16].

v^2/c^2 , of 0.68 rather than the theoretical prediction of $k = 0.5$. The explanation of Kholmetskii et al. is that the constant k may be affected by experimental effects. That is, that the behavior of k is affected by the experimental conditions themselves, like, for example, vibrations in the apparatus. With this possibility, it could be the case that these higher order terms could contribute more to the Doppler shift observed in the recoil of the nucleus. This is a problem that is still unsolved, because of the difficulty of reducing the experimental apparatus vibration to zero in real experiments and apparatus.

1.4 The Mössbauer Effect at Houghton College

Taking inspiration from the previous experiments [6, 12-14] Houghton College began an experiment to demonstrate general relativity by using the transverse Doppler effect. The focus has so far been on

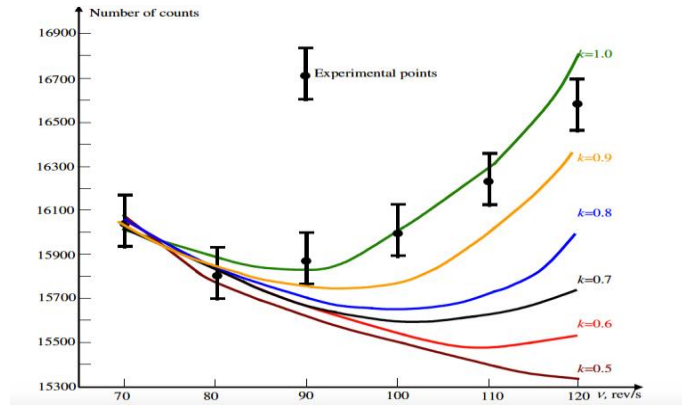


Figure 10. Kolmetskii et al. $\text{K}_4\text{Fe}(\text{CN})_6 \cdot 3\text{H}_2\text{O}$ absorber results. The best fit to experimental data points for the second order relativistic Doppler shift is $k = 1.0$. Figure taken from Ref. [16].

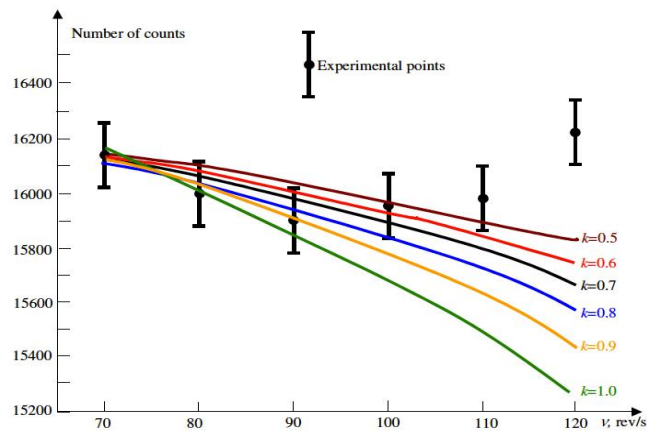


Figure 11. Kolmetskii et al. $\text{Li}_3\text{Fe}_2(\text{PO}_4)_3$ absorber results. The best fit to experimental data points predict for the coefficient of the second order relativistic Doppler shift is $k = 0.5$. Figure taken some Ref. [16].

producing low activity Mössbauer sources by electroplating and then subsequent diffusion of the source into a crystal lattice by heating the lattice material in a vacuum furnace.

Because of licensing requirements, Houghton has historically used exempt sources on the order of $1 \mu\text{Ci}$. These sources are several orders of magnitude less active than previous Mössbauer experiments [6, 12-14]. The sources purchased come in solution form, which is ideal for electroplating; these sources were purchased from Spectrum Techniques [17].

The experiment involves electroplating ^{57}Co dissolved in an HCl solution onto a stainless steel foil. In doing this, additional ^{59}Co is introduced to aid the process of electroplating. Several alloys of 0.001 inch thickness steel foils in the 300 series have proven to be good electroplating substrates.

In order to create a Mössbauer source, the ^{57}Co needs to be diffused into the steel foil, which requires heating the substrate. These substrates are placed into a vacuum furnace to diffuse the ^{57}Co into the lattice. The source obtained is then placed in the experimental apparatus.

The decay scheme of ^{57}Co is shown in Figure 12. The most likely decay chain, occurring approximately 86% of the time, produces a cascade of a 122.1 keV and a 14.4 keV gamma ray. A NaI detector will detect the 122.1 keV gamma ray in coincidence with the 14.4 keV gamma ray detected by a CdTe X-ray detector.

Two experiments are to be conducted, the longitudinal Doppler effect and the transverse Doppler effect. The longitudinal Doppler effect, shown in Figure 13, will be used to test the Mössbauer sources. The main experiment to measure the transverse Doppler effect is intended to demonstrate general relativity. This latter experiment requires that the disk shown in Figure 13 be perpendicular to the line made by the faces of the two detectors. The transverse Doppler effect apparatus is shown in Figure 14.

For the longitudinal Doppler effect, the absorber disk is angled relative to the line connecting the source and the X-ray detector. The 14.4 keV gamma rays will either pass through the disk and may be detected or they may be absorbed by the iron on the face of the disk if the disk is spinning at the correct speed to cause the needed longitudinal Doppler shift. The 122.1 keV gamma rays that go into the NaI detector may be detected in coincidence with the 14.4 keV gamma ray in the CdTe detector. This allows for a reduction in the background allowing us to use a very weak source, since we only look for the 14.4 keV gamma ray when we know one will be released in cascade with the 122.1 keV gamma ray.

For the transverse Doppler effect, as with the longitudinal Doppler effect, the source and detectors will be positioned as close as possible to the rotating disk. Since the number of counts will go down as $1/r^4$ the ^{57}Co source will be attached to the face of the NaI detector, so that roughly 50% of the 122.1 keV gamma rays will go into the NaI detector to trigger coincidence electronics with the 14.4 keV gamma ray. The velocity of the absorber must be perfectly transverse to the source such that there is no longitudinal component of the Doppler shift, but only the relativistic transverse Doppler effect

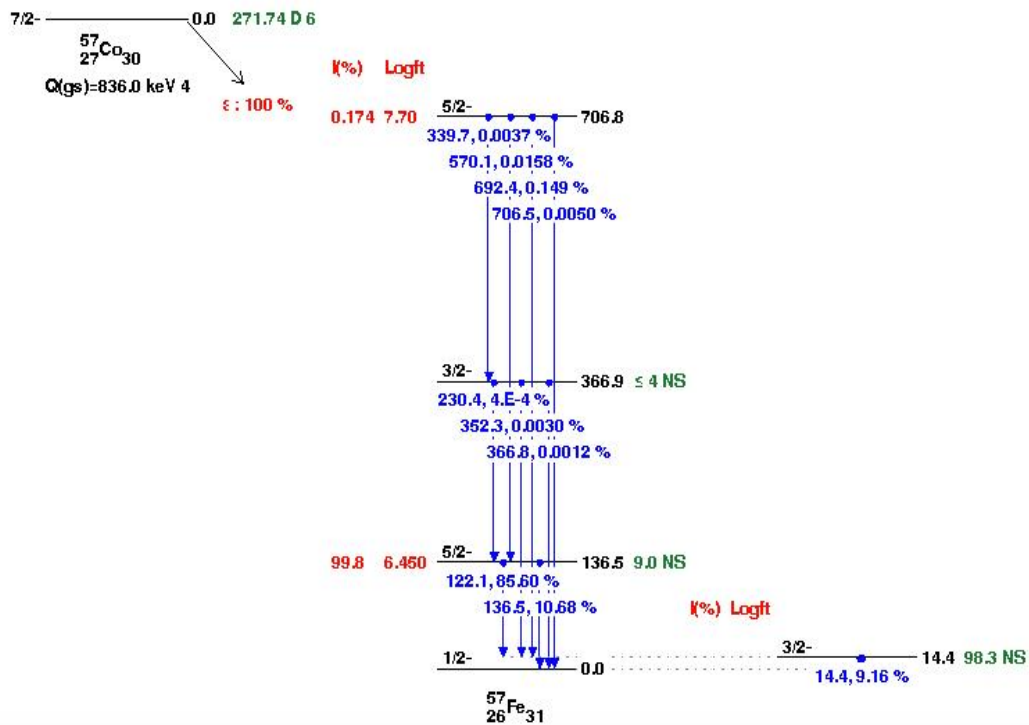


Figure 12. The Decay Scheme of ^{57}Co . The ^{57}Co decays by electron capture 100% of the time and 99.8% of the time enters the 136.5 keV energy level. There is a small, 10.68%, chance of decaying straight into the ground state. There is an 85.6% chance for the 122.1 keV gamma ray to be emitted and then subsequently the 14.4 keV gamma ray. Figure taken from Ref. [16].

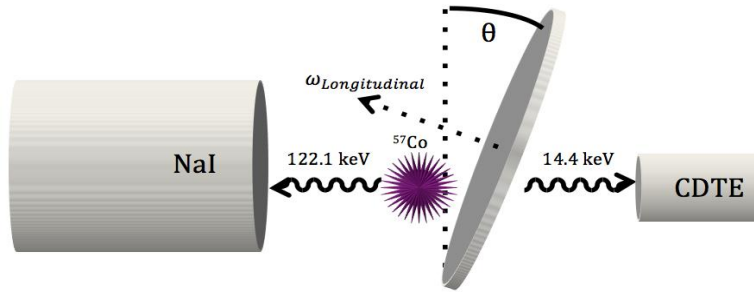


Figure 13. Longitudinal Doppler effect apparatus. The absorber disk is angled with respect to the line connecting the source and the X-ray detector to allow the longitudinal Doppler effect to occur. The source and detectors will be positioned as close as possible to the rotating disk. The 122.1 keV gamma rays that go into the NaI detector triggers the electronics in coincidence with the 14.4 keV gamma ray. The 14.4 keV gamma ray will either pass through the disk or be absorbed. By varying the speed of the disk and scanning through the resonance spectrum, nuclear resonance fluorescence will be observed.

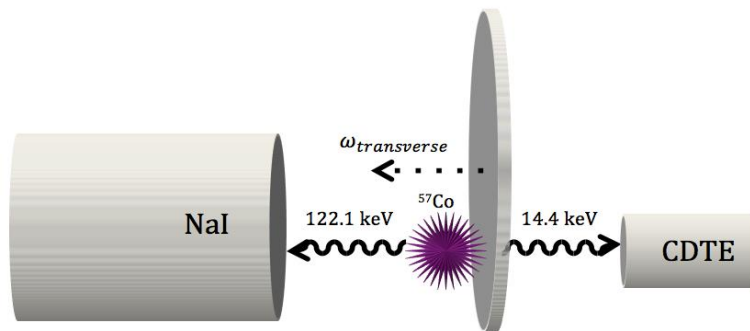


Figure 14. Transverse Doppler effect apparatus. The disk is positioned such that velocity of the absorber is transverse to the source. The speed, is on the order of tens of thousands of revolutions per minute. In the frame of the disk, if the correct speed is achieved the frequency of clocks of the ^{57}Fe nuclei are slowed, and thus they are able to see the incoming 14.4 keV gamma ray shifted such that nuclear resonance fluorescence can occur.

2.1 Nuclear Resonance Fluorescence

Resonance fluorescence is the emission and subsequent reabsorption of a characteristic photon, as shown in Figure 1. For atomic resonance fluorescence, an excited atom will decay by emitting a photon. That photon can then be reabsorbed by another identical atom. This process can then be repeated, as shown in Figure 15.

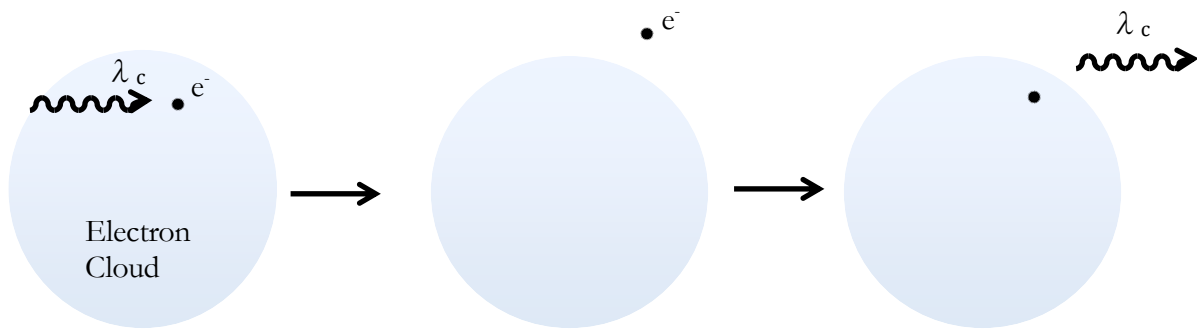


Figure 15. Atomic resonance fluorescence. A photon of the characteristic wavelength excites an atom into a higher energy state. That excited atom can then de-excite and emit a photon with the same wavelength as was previously absorbed. That emitted photon can then cause subsequent resonant fluorescence to occur if it excites another atom.

Similar to atomic resonance fluorescence, nuclear resonance fluorescence is the emission of a gamma ray from an excited nucleus and the consecutive absorption and re-emission of the characteristic

gamma ray. However, nuclear resonance fluorescence was not observed for many years because of nuclear recoil [6], which causes the gamma ray to lose energy because of the Doppler effect.

2.1.1 Recoil vs. Recoilless Emission

Nuclear resonance fluorescence was not initially detected due to the loss of energy of the recoiling nucleus. Consider a free excited nucleus. When that nucleus eventually decays it is required, by conservation of momentum, to recoil in the opposite direction of the emitted gamma ray. That is, from conservation of momentum, we have,

$$\vec{P}_R + \vec{P}_\gamma = 0 \quad (2.1)$$

where \vec{P}_R is the momentum of the recoiling nucleus and \vec{P}_γ is the momentum of the emitted gamma ray. So, it follows that

$$\vec{P}_\gamma = -\vec{P}_R. \quad (2.2)$$

Clearly the magnitudes of these quantities are the same, thus,

$$P_\gamma = MV_{\text{Nucleus}} \quad (2.3)$$

where M is the mass of system of which the nucleus is a part and V_{Nucleus} is the velocity of the recoiling nucleus. It is clear then that if the mass M grows, possibly even becoming as large as the entire crystal lattice, then to maintain the equality the velocity of the recoiling nucleus, V_{Nucleus} , must be reduced. It would be the ideal case if V_{Nucleus} could be essentially reduced to zero by placing the parent nucleus into a massive lattice to absorb the momentum. So, by employing a crystal lattice as a carrier for the decaying parent nucleus, one could use this effect, the Mössbauer effect, to reduce the recoil and to allow for the possibility of nuclear resonance fluorescence. What is the difference between recoil and recoilless emission? It is the difference between the nuclear recoil energy being

absorbed by a massive substrate lattice or a free nucleus. The value of M is the key difference between recoil emission and recoilless emission.

2.1.2 Conservation of Energy

A simple analysis of the decaying nuclear systems using conservation of energy yields,

$$E_r = E_\gamma + E_R \quad (2.4)$$

where E_R is the energy of the recoiling nucleus, E_γ is the energy of the emitted gamma ray, and E_r is the energy released by the de-excitation. The classical kinetic energy of the recoiling nucleus can be written in terms of the momentum, using Eq. 2.2 then yields,

$$E_R = \frac{P_R^2}{2M} = \frac{P_\gamma^2}{2M} = \frac{E_\gamma^2}{2Mc^2}. \quad (2.5)$$

This analysis assumes that the recoiling system can be treated non-relativistically, which is true if $E_R \ll Mc^2$, a valid assumption for most nuclear systems used in Mössbauer experiments. As an example for ${}^{57}_{26}\text{Fe}$, $Mc^2 \approx 54 \text{ GeV}$ and $E_R \approx 0.002 \text{ eV}$ [6].

2.1.3 Mean Line Width

Nuclear decay gamma ray spectral lines are mathematically described by Breit-Wigner distributions. These distributions have the form,

$$\sigma_R(E) = \frac{4\pi}{P_\gamma^2} (2l + 1) \frac{\left(\frac{\Gamma^2}{4}\right)}{(E - E_\lambda)^2 + \left(\frac{\Gamma^2}{4}\right)} \quad (2.6)$$

where σ_R is the cross section of the resonance absorption, l is the angular momentum quantum number, E_λ is the transition energy of the decay of the ${}^{57m}_{26}\text{Fe}$ excited state, and Γ is the mean line width. This equation represents the probability of absorption as a function of energy.

The mean line width, or the FWHM of the Breit-Wigner energy distribution about the resonant energy, that is in our case $^{57m}_{26}\text{Fe}$, arises from the Heisenberg uncertainty principle,

$$\Delta E \Delta t \geq \frac{\hbar}{2} \quad (2.7)$$

where ΔE is the standard deviation from the mean energy of the transition, and Δt is the standard deviation in time, the lifetime of the excitation state. This relationship tells us that the mean line width can be expressed as a function of the width of the lifetime Δt . Therefore, since the standard deviation for this distribution is one half of the line width, this ΔE can be expressed in terms of the line width as,

$$\Delta E = \frac{\Gamma}{2} \quad (2.8)$$

where Γ is the mean line width, that is, the FWHM of the Breit-Wigner distribution about the mean transition energy. From Eq. 2.7 then, the standard deviation of the lifetime Δt is the mean lifetime. Thus,

$$\tau \geq \frac{\hbar}{\Gamma} \text{ and } \Gamma \geq \frac{\hbar}{\tau} \quad (2.9)$$

For ^{57}Fe , $\tau = 98.3 \text{ nsec}$ is the mean lifetime for the 14.4 keV decay [18], so

$$\Gamma_{^{57m}_{26}\text{Fe}} \geq 6.967 \times 10^{-9} \text{ eV}. \quad (2.10)$$

This is the FWHM of the Breit-Wigner distribution of the gamma ray energy for the 14.4 keV gamma ray line that is emitted in coincidence with the 122.1 keV gamma ray decay after the electron capture decay of ^{57}Co , as was shown in Figure 12.

2.1.4 Doppler Broadening

In addition to the intrinsic line width described above, the width of the gamma ray line is also broadened by the thermal motion of nucleus itself before the emission of a gamma ray. It has been assumed up to this point that both the source and absorber are stationary; that is, there has been an assumption that the nuclei have no kinetic energy. However, the decaying nucleus has thermal energy so this is obviously an incorrect assumption. Returning to Eq. 2.4 we find then that the energy that is lost from the gamma ray in recoil is now given as,

$$E_{R'} = \frac{P_R^2}{2M} = \frac{(\vec{P}_i - \vec{P}_\gamma) \cdot (\vec{P}_i - \vec{P}_\gamma)}{2M} - \frac{P_i^2}{2M} \quad (2.11)$$

where $E_{R'}$ is the energy of the recoiling nucleus with the Doppler broadening included, and \vec{P}_i is the momentum carried by the nucleus in thermal motion before the emission of the gamma ray. By performing the inner product of the first term, it is found that

$$E_{R'} = \frac{P_\gamma^2}{2M} - \frac{P_i P_\gamma}{M} \cos(\phi) \quad (2.12)$$

where ϕ is the angle between the direction of the emitted photon and the thermal motion of the nucleus. If we let

$$D = 2 \left(\frac{P_i^2 P_\gamma^2}{2M 2M} \right)^{\frac{1}{2}} \quad (2.13)$$

then Eq. 2.12 becomes,

$$E_{R'} = E_R - D \cos(\phi). \quad (2.14)$$

This Doppler broadening changes the energy of the emitted gamma ray by either increasing the recoil energy or reducing it, that is, by having the nucleus moving away or towards, respectively, the direction of motion for the gamma ray. So, we find that the energy of the gamma ray is given by,

$$E_{\gamma} = E_r - E_{R'}, \text{ or}$$

$$E_{\gamma} = E_r - E_R + D\cos(\phi). \quad (2.15)$$

This effect, because the direction of travel before emission is random, causes the broadening of the peaks shown in Figure 16 to have a bell-shaped distribution about the mean.

2.2 What Makes a Good Absorber?

There are several properties that make an absorber work well for experiments using the Mössbauer effect. The first, the line width, is a measure of how sharp the Breit-Wigner distribution is. Second is the natural abundance of the stable absorber isotope. Third is a large cross-section for the absorption of the excitation gamma ray. Finally, the energy loss due to recoil which is based on the mass of the isotope and the energy of the emitted gamma ray, refer to Eq. 2.5 [8]. These properties widely vary from isotope to isotope, however, it is desired that the line width be small on the order of 10^{-9} eV or less, an appreciable percentage of natural abundance $>1\%$, a high absorption cross section in the region of kbarns or higher, and a low recoil energy of 10^{-2} eV or less. For ^{57}Fe these properties are,

$$\Gamma_{57mFe} \geq 6.967 \times 10^{-9} \text{ eV} \quad (2.16)$$

$$(^{57}\text{Fe})_{\text{natural abundance}} = 2.17\% \quad (2.17)$$

$$\sigma_{14.4 \text{ keV}} = 2.26 \text{ Mbarns} \quad (2.18)$$

$$E_R = \frac{E_{\gamma}^2}{2M_{^{57}\text{Fe}}c^2} = 1.955 \text{ meV} \quad (2.19)$$

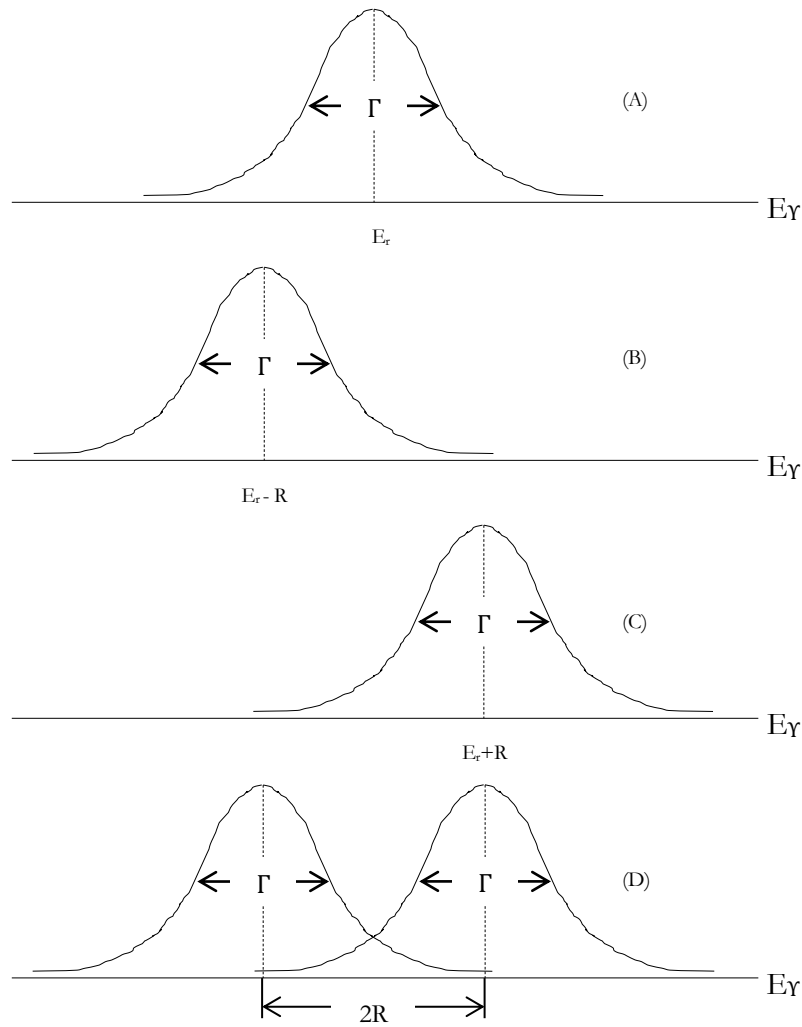


Figure 16. Overlap of the Breit-Wigner distributions. In (A) the energy of the emitted gamma ray is centered around the resonant transition energy E_r . Then, in (B) the Breit-Wigner distribution is shifted to a lower energy than resonant transition energy due to the energy loss caused by the transfer of momentum into the recoiling nucleus E_R . In (C) the absorbing nucleus requires the transition energy as well as the recoil energy. The two distributions in (D) show that when the recoil energy E_R is low enough the Breit-Wigner distributions begin to overlap again and allow for resonance fluorescence to occur. Figure taken from Ref. [3].

2.3 Relativistic Doppler Effects

Suppose there is light wave and there are two observers, one in a frame S and another in a frame S' with a boost \vec{v} in the +x direction. This is shown in Figure 17. This wave is expressed, in the S frame, as

$$\vec{E} = \vec{E}_0 \cos(\vec{k} \cdot \vec{r} - \omega t) \quad (2.20)$$

where E is the electric field strength of the wave of light, \vec{k} is the wave vector pointed in the direction of propagation in the S frame and is expressed as $\vec{k} = k_x \hat{x} + k_y \hat{y}$, \vec{r} is position vector in the S frame, and ω is the frequency of the wave in the S frame. Since all observers must agree on the phase of the

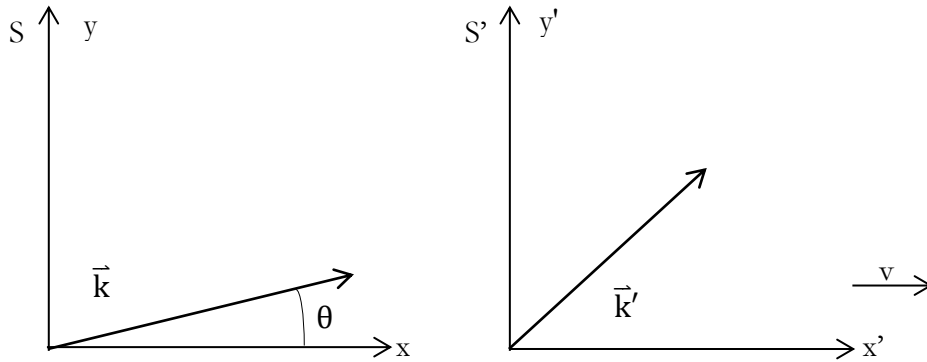


Figure 17. Relativistic effects on light. A wave of light propagating in space is observed by two observers, one in the lab frame S and another in a moving frame S'. Both observers agree on the phase of the light, however the frequency recorded by each observer is affected by the velocity of the S' frame.

wave the quantity $\vec{k} \cdot \vec{r} - \omega t$ must be an invariant quantity, so,

$$\vec{k}' \cdot \vec{r}' - \omega' t' = \vec{k} \cdot \vec{r} - \omega t. \quad (2.21)$$

Through the Lorentz transformation to the S' frame,

$$k'_x = \gamma \left(k_x - \frac{\omega v}{c^2} \right), \quad (2.22)$$

$$k'_y = k_y, \quad (2.23)$$

and

$$\omega' = \gamma(\omega - vk_x). \quad (2.24)$$

Suppose we let $k_y = 0$. If so, from Figure 17, it is shown that the light is only traveling in a direction parallel to the boost. By doing this, the effects on the frequency due to the relativity in the S' frame can be determined. Because $k^2 = k_x^2 + k_y^2 = \frac{\omega^2}{c^2}$, $k_x = \frac{\omega}{c}$, it is then shown from Eq. 2.24,

$$\omega' = \gamma\omega(1 - v/c), \quad (2.25)$$

and therefore,

$$\omega = \omega' \sqrt{\frac{(1 + \beta)}{(1 - \beta)}}. \quad (2.26)$$

This is the relativistic longitudinal Doppler effect. Now, suppose that $k'_x = 0$ instead, by doing so, the observer in S' will record the frequency shift of the light due to the transverse propagation of the light. In the S frame, the light propagates at an angle θ with components of,

$$k_y = \frac{\omega}{c} \sin \theta, \quad (2.27)$$

$$k_x = \frac{\omega}{c} \cos \theta. \quad (2.28)$$

Substituting k_x into Eq. 2.22 and solving for $\cos \theta$,

$$\cos \theta = \beta. \quad (2.29)$$

Then solving for the relationship between ω and ω' , from Eq. 2.24,

$$\omega = \gamma \omega'. \quad (2.30)$$

This is the relativistic transverse Doppler effect. The relativistic transverse effect produces a frequency shift proportional to the Lorentz-factor.

2.3.1 Calculating the Longitudinal Rotation Speed for the Absorber

The necessary rotation speed for the longitudinal Doppler effect absorber is derived from the relativistic Doppler effect,

$$\omega = \omega' \left(\frac{\sqrt{1 + \beta}}{\sqrt{1 - \beta}} \right) \quad (2.31)$$

where ω is the frequency of the observed nuclear radiation, ω' is the frequency observed in the rest frame of the emission, and β is v/c . Multiplying by Planck's constant, and then using the binomial expansion yields,

$$E \cong E_\gamma \left(1 + \frac{v}{c} + \frac{1}{2} \left(\frac{v}{c} \right)^2 + \dots \right) \quad (2.32)$$

where E is the energy of the gamma ray as observed, and v is the longitudinal component of the absorber's velocity in the direction antiparallel to the propagation of the gamma ray. Now, since the

velocities which cancel the recoil are on the order of 1×10^{-4} m/sec, the second order and higher terms are negligible. So, Eq. 2.32 can be rewritten as,

$$v = \frac{\Delta E}{E_\gamma} c \quad (2.33)$$

where $\Delta E = E - E_\gamma$ is the difference in energy due to the Doppler shift, which, we have seen before in Eq. 2.16. So, everything that is needed to solve this for ^{57}Co has been found to this point, thus, a typical longitudinal component of the absorber velocity is

$$v = \frac{\frac{1}{2} (6.967 \text{ eV}) (3 \times 10^{-1} \frac{\text{m}}{\text{s}})}{14.4 \text{ eV} \times 10^3} = 7.26 \times 10^{-5} \frac{\text{m}}{\text{s}} \quad (2.34)$$

2.3.2 The Transverse Doppler Effect

The relativistic transverse Doppler effect is the Doppler effect experienced by an observer moving perpendicular to the motion of a source object. Therefore an incoming gamma ray would see, from its frame of reference, that an absorber traveling transverse to its approach, and therefore, that the clock of the absorber had slowed down. It therefore records that the frequency necessary to excite this nucleus is lower than that which a gamma ray in the frame of the absorber would record. This frequency would be,

$$\omega = \gamma \omega' \quad (2.35)$$

where ω is the frequency observed in the frame of the source, ω' is the frequency observed in the frame of the absorber, and γ is the Lorentz factor. Now, the energy can be expressed as,

$$E = \hbar \omega \quad (2.36)$$

where E is the energy of the gamma ray in the same frame as that of the frequency, ω . Therefore,

$$E = \gamma E', \quad (2.37)$$

and since ΔE is,

$$\frac{\Delta E}{E} = \frac{E' - E}{E} \quad (2.38)$$

where E' is the energy of the gamma ray as recorded by the absorber, and E is the energy as recorded by the rest frame of the gamma ray. From Eq. 2.35 and Eq. 2.36, Eq. 2.38 can be expressed as,

$$\frac{\Delta E}{E} = \frac{\omega'}{\omega} - 1 = \sqrt{1 - \beta^2} - 1. \quad (2.39)$$

By expanding the first term using the binomial expansion,

$$\frac{\Delta E}{E} \cong \left(1 + \frac{1}{2}(-\beta^2) \right) - 1 \quad (2.40)$$

where higher order terms of the expansion are neglected since we assume $\beta \ll 1$. Therefore, the transverse Doppler shift is given by,

$$\frac{\Delta E}{E} \cong -\frac{1}{2}\beta^2. \quad (2.41)$$

Which, if we were to calculate the necessary velocity of the absorber, it would be approximately,

$$v \cong \sqrt{\frac{\left(2 \left(\frac{6.967}{2} \times 10^{-9} \text{ eV} \right) \left(3 \times 10^8 \frac{\text{m}}{\text{s}} \right)^2 \right)}{14.4 \times 10^3 \text{ eV}}} \quad (2.42)$$

$$v \cong 208.67 \frac{\text{m}}{\text{s}}. \quad (2.43)$$

For a rotating wheel with a 10 cm radius,

$$\omega \cong \frac{v}{r} = \frac{208.67 \frac{\text{m}}{\text{s}}}{0.1 \text{ m}} = 2086.7 \frac{\text{rad}}{\text{s}} = 19926.52 \frac{\text{rev}}{\text{s}}. \quad (2.44)$$

As mentioned previously in Sections 1.2 and 1.3, the thermal energy of the parent nucleus and daughter nucleus absorber is critical. Even slight changes in thermal energy can broaden the peaks and cause overlap. This shift can be explained in terms of the relativistic second order Doppler shift,

$$\frac{\Delta E_{\text{thermal}}}{E_{\gamma}} = \frac{1}{2c^2} (\langle v_s^2 \rangle - \langle v_a^2 \rangle) \quad (2.45)$$

where $\Delta E_{\text{thermal}}$ is the change in energy of the gamma ray due to thermal energy, E_{γ} is the energy of the gamma ray, and v_s and v_a are the velocity of the source and the absorber. For a monatomic solid with harmonic lattice forces,

$$\frac{1}{E} \frac{\partial E}{\partial T} = \frac{-C_p}{2c^2}. \quad (2.46)$$

where C_p is the specific heat of the lattice of the source. For iron the shift observed was $(-2.09 \pm 0.05) \times 10^{-15} K^{-1}$ [19].

2.4 Gravitational Redshift

Another way to show the same effect shown above, as occurring due to the transverse Doppler effect, is via the gravitational redshift of the gamma ray. From the standpoint of general relativity, an acceleration is equivalent to a gravitational field. This is the equivalence principle. Thus, consider an observer of mass m on a rotating disk at a radius R . They would observe the following,

$$a_c = \frac{v^2}{R} = \frac{(R\omega)^2}{R} \quad (2.47)$$

where \mathbf{a}_c is the radial acceleration of the observer toward the center due to the rotation of the disk, \mathbf{v} is tangential velocity of the observer as recorded by the lab frame, and $\boldsymbol{\omega}$ is the angular velocity of the observer as recorded in the lab frame. The force acting on the observer would therefore be,

$$\mathbf{F} = m\mathbf{a}_c = mR\boldsymbol{\omega}^2 \quad (2.48)$$

so that the potential energy would be the work require to move from the center to radius R is

$$V = \int_0^R mr\boldsymbol{\omega}^2 dr. \quad (2.49)$$

The gravitational potential would therefore be,

$$\Phi = \frac{V}{m} = \frac{1}{2}R^2\boldsymbol{\omega}^2. \quad (2.50)$$

Now, the gravitational redshift of the observer is,

$$\Delta E = -m\Phi, \quad (2.51)$$

Therefore the relative shift in energy is,

$$\frac{\Delta E}{E} = -\frac{m\Phi}{mc^2} = -\frac{(R\boldsymbol{\omega})^2}{2c^2} = -\frac{1}{2}\beta^2. \quad (2.52)$$

Thus, the transverse Doppler shift in the frame of the source is the same as a gravitational redshift due to the gamma ray gaining potential by falling into the gravitational potential well of the rotating disk from the absorbers frame.

Chapter 3

EXPERIMENT

3.1 Making a Mössbauer Source

The greatest difficulty in this experiment has been creating low activity Mössbauer sources. The procedure requires that the steel foil used, in our case type 302 stainless steel, be very clean. The impurities that are of greatest concern, due to their ability to inhibit the electroplating and diffusion process, are organics, oils and biomaterials, and inorganics such as tarnishing and rust. There are four layers to the foil, particulates, including dust, lying atop organic materials, such as oils and biofilms, possibly mixed amongst inorganic materials, such as oxidation layers, and then the foil itself. In order to remove these extra layers a cleaning process must be employed.

After cleaning a foil of these contaminants, the foil was used as an electroplating substrate. By providing a potential difference across a radioactive solution containing ^{57}Co , the ^{57}Co ions were attracted to the foil and were electroplated.

In addition to the benefits of cleaning for electroplating, it also aided the diffusion process. In this process, the foil was heated inside of a vacuum chamber to embed the ^{57}Co atoms into the steel lattice. This process, as discussed more in Section 3.1.6, was used to create a Mössbauer source from the electroplated substrate.

3.1.1 Contamination Prevention

At the outset of cleaning the foil, the organics and surface particulates were eliminated. First, to keep from spreading organic contamination, rubber gloves were employed. To prevent the gloves themselves from being contaminated with oils and particulates, isopropanol and distilled (DI) water were used to remove oils and particulates from the gloves, respectively. Since each door, table, and surface used could contain particulates and/or oils, it was necessary to cleanse the gloves again after

touching such a surface or to save one glove, in one hand, which was designated to interact with the foil.

3.1.2 Removing Particulates and Organic Materials

By using DI water first, the first layer, dust and other particulates were removed from the surface. Then by the use of isopropanol any oils that accumulated on the surface of the steel foil were removed by isopropanol breaking down the oils. Isopropanol could introduce another layer of particulates though, so it was necessary to rinse once more with DI water. This cleanses, for the most part, the foil of particulates and oils.

3.1.3 Removing Inorganic Materials

Afterward, in order to remove the inorganic compounds from the face of the steel plate, a strong inorganic acid was used. In order to prevent recontamination due to introducing oxidizing agents, most importantly oxygen, using an acid like HCl that does not contain oxygen was necessary. Because the 300 series stainless steel foils are designed to resist tarnishing and oxidation by containing chromium which forms the Cr-O bond instead of the Fe-O bonds, the step of rinsing the foil in HCl may harm the foil. This is because the bond of Cr-O is stronger than Cr-Cl, so oxygen cannot be removed from the chromium bonds on the surface of the plate. However, if there are impurities, Fe-O bonds, or metallic dust on the face of the plate the HCl rinse will remove these effectively.

3.1.4 Mixing the Radioactive Solution

Once a steel foil substrate was cleaned, a ^{57}Co solution was prepared using the manufacturer's source bottle containing the ^{57}Co in solution form, as well as a destination source bottle; that is, two bottles were used to prepare the solution for electroplating; the source was purchased from Spectrum Techniques [17]. It was necessary to use plastic gloves here as well, because the measurements being taken were small enough that fingerprints, that is the oils left behind, would increase the mass of the source bottle enough to change the results of the experiment. A measurement of the mass of the bottle with the ^{57}Co solution was essential for the analysis of the amount of ^{57}Co electroplated to the foil.

On the lid of the source bottle containing the ^{57}Co , there was a tape around the lip of the new source bottle. This tape was removed before massing the container with the solution. Once removed, the source bottle, including the cap, was placed into a Mettler and Toledo MS 104S/03 Analytical Balance. The mass was recorded before the next step of adding an HCl mixture. The approximate activity of the source, provided by the manufacturer, was $1.0 \pm 0.2 \mu\text{Ci}$. This value, converting the number of atoms to mass using the molar mass of ^{57}Co , is $1.185 \times 10^{-10} \pm 2.37 \times 10^{-11} \text{ g}$ of ^{57}Co . The molar mass of ^{57}Co is 56.936296 g/mole.

Next, in a beaker, a sufficient amount of HCl was measured out to add to the source bottle containing the ^{57}Co source. The value that has worked in the past tends to be around 1.8 g of 0.1M HCl. After this amount was massed out into a beaker, the HCl was pipetted into the source bottle. The source bottle was massed again to reflect the addition of the HCl. This was recorded before the ^{59}Co was mixed into the source solution. In the past a concentration near 0.5 M of Co in solution was used.

A compound containing ^{59}Co , specifically $^{59}\text{CoCl}_2 \cdot 6\text{H}_2\text{O}$, that dissolves in the HCl present in the source bottle was used to supplement the amount of ^{57}Co present in the source solution. This is necessary because, in order to electroplate effectively, a sufficient number of cobalt ions must be present to produce the electroplating behavior we seek. That is, if there are very few ions of cobalt within the solution, the rate of electroplating is slower than the rate at which the HCl removes ions from the steel substrate.

3.1.5 *Electroplating*

The electroplating apparatus at Houghton College, shown in Figure 18, was a simple glass T used to hold a ^{57}Co solution over the steel foil and a platinum wire that was inserted into the glass T arm to use as a cathode. The cylindrical dimensions of the glass T to hold the solution were a 6mm diameter and a height of 20 mm, allowing for a solution volume of about 0.57 mL. The length of the arm to hold the platinum cathode was 47.5 mm in order to keep the platinum cathode wire in the solution but not touching the steel foil. The platinum cathode was mounted in a glass cap. The foil, like the platinum

wire, was connected to a HY3003-3 DC Power Supply, using the circuit shown in Figure 19. The foil was approximately 26 mm by 13.5 mm.

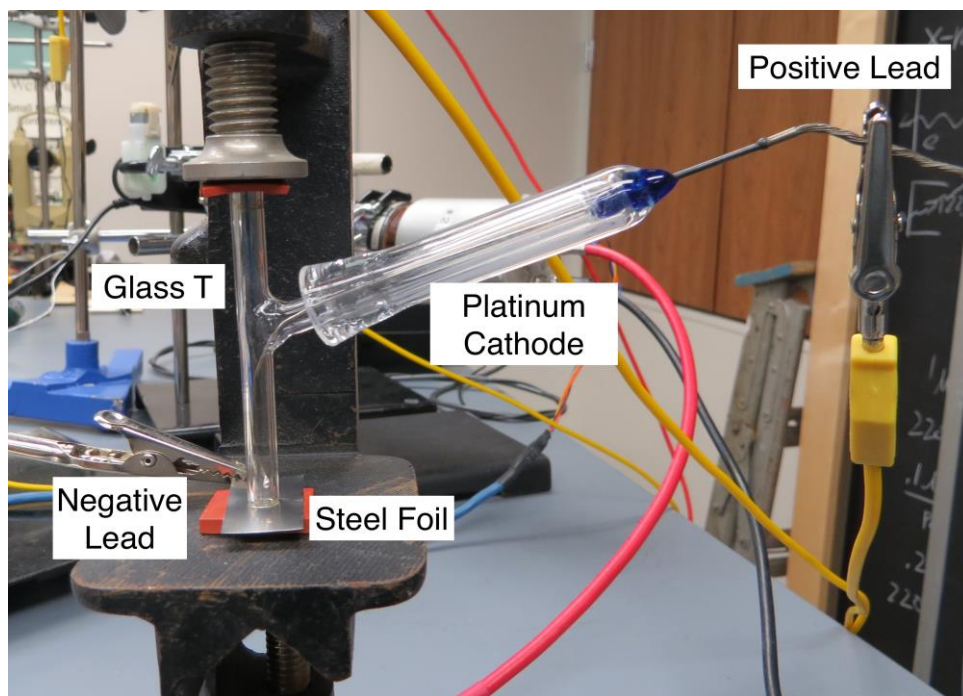


Figure 18. Electroplating apparatus. The radioactive solution fills the glass-T up to the shoulder of the raised arm. The cathode was placed into the glass-T and a potential difference around 3.75 V was placed across the leads.

Once the foil was cleansed of the impurities mentioned above and a solution was made, a ^{57}Co source was electroplated onto the steel foil. Once the glass-T was pressed against the foil using a clamp to gently tighten the glass-T in place, about 0.57 mL of radioactive solution was inserted into the glass-T, filling the T column up to the shoulder. The platinum cathode was placed in and adjusted to an appropriate height, which was around 10 mm from the foil. The cathode was connected to the positive lead from a Mastech HY3003-3 DC Power Supply, which was set to a voltage between 3.5-4 V. The negative lead was connected to the foil through a Mastech MS8050 Digital Multimeter in order to

measure the current. The output is sent via the RS232 to a computer, which then, using the MS8050 software, recorded the data into a .CSV format to be analyzed.

Bubbles appearing within the solution signaled that the electroplating process was occurring. These bubbles were the release of chlorine from the solution. It was a problem in the past that the solution needed to be stirred during the electroplating process to prevent bubbles inside of the apparatus from reducing the current. However, by using the less concentrated solution of 0.5M and lower voltages of 3.5-4 V, the need to stir the solution was reduced.

Once the electroplating process began it took around 3-4 hours to finish. During this time, the data read out from the MS8050 Digital Multimeter was stored in .CSV format. The MS8050 Digital Multimeter sampled the current every half second. A plot of the current versus time is shown in Figure 20.

3.1.6 Diffusion of ^{57}Co

Once the electroplating process was completed the ^{57}Co was diffused into the steel lattice. The furnace, which the foil was placed into, was pumped down to about 10^{-6} Torr before heating the foil. This furnace is shown in Figure 21. The vacuum chamber was pumped down to this pressure in order to prevent the oxidation of the foil when heated to 1000 °C. The pressure was monitored by a

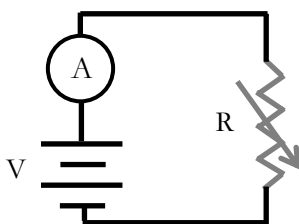


Figure 19. Electroplating circuit diagram. A potential difference was placed across the radioactive solution and ions then drifted in solution and produced a current. This current was recorded and output from the RS232 capabilities of the MS8050 Digital Multimeter.

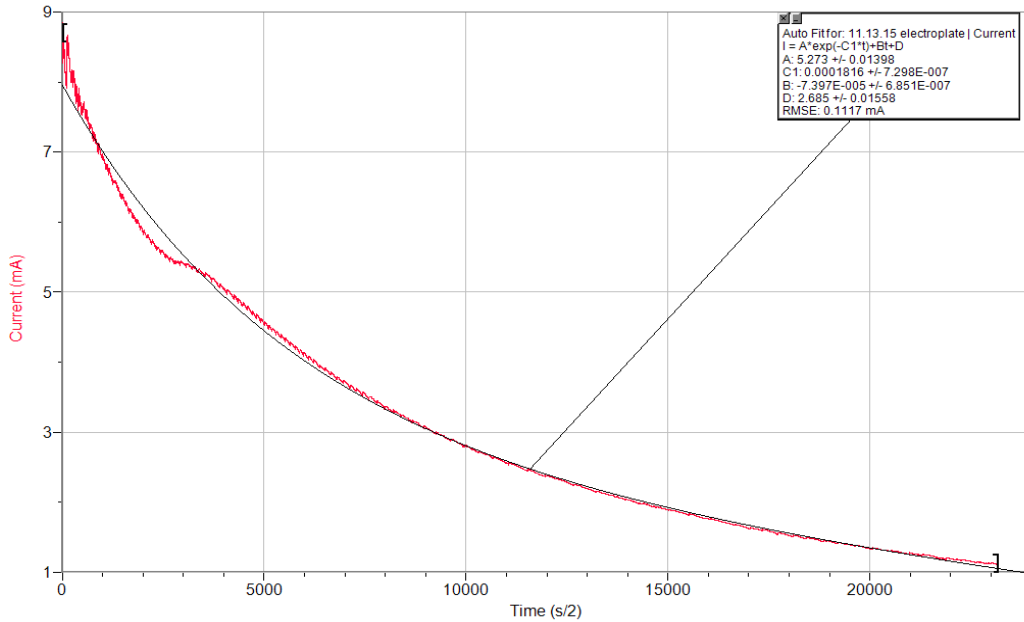


Figure 20. Electroplating current versus time data. The current versus the time of the electroplating run performed on 13 November 2015. The fit of the data is $I = A \exp(-Ct) + Bt + D$. By integrating the $A \exp(-Ct)$ portion of the fit, the total charge of the ^{57}Co ions electroplated was obtained and thus the total number of ^{57}Co nuclei that were deposited.

Stanford Research Systems Model IGC100 Ion Gauge Controller reading out a Duniway Stockroom Corporation I-100-K Ion Gauge. This low pressure was necessary because oxygen could bind to the surface of the foil while heating and could prevent the cobalt atoms from diffusing.

Once this pressure was reached, a Mastech HY1550EX DC Power Supply was used to heat the foil. The foil was attached to two copper rods which acted as a rigid mount for the foil as well the leads to pass current through the foil the heat it. A current from 1.5 A to 28 A was used to reach the temperatures necessary, increasing from 1.5 A using 1 A or 0.5 A steps. A record of the temperature of the plate as recorded by the temperature sensor versus the current is shown in Figure 22. At the same time, a Metex M-4650 Digital Multimeter was used to measure the potential difference across the leads. From these measurements, the resistivity of the plate was calculated. A figure of this apparatus is shown in Figure 23. Resistivity measurements are shown in Figure 24. The critical temperature sought

is 1000 °C. This is the temperature at which the cobalt begins to diffuse into the substrate of the steel lattice and before the iron and cobalt melted at 1538 °C and 1495 °C, respectively. In order to measure the temperature, a Cheerman DT8011 Temperature Sensor was used. This device measures the flux of infrared radiation and converts the flux measured to an electrical signal to display the temperature. In order to protect the optical sensors of the temperature sensor from the sputtering steel foil, an aluminum arm was attached to a valve in line with the foil. This is shown in Figure 25. Once this critical temperature was reached, the foil was left to diffuse for 2 hours.

3.2 Vacuum System

The furnace used a vacuum chamber of volume roughly 300 in³ it was first pumped down using a fore-pump to pressures in the 10⁻² Torr range as measured by a Model KJL275806 Kurt J. Lesker Pirani Pressure Gauge. A Kurt J. Lesker TNR6XA150QF diffusion pump was then used to reduce the pressure to the range of 10⁻⁵ – 10⁻⁶ Torr. In order to remove water molecules in the vacuum chamber a LN2 cold trap was used. A heater tape allowed the chamber to be heated, causing the outgassing of water molecules from the walls. Once these methods have been used and the system is allowed to evacuate over a period of 12 hours or more a pressure on the order of 10⁻⁶ Torr was reached.

3.3 Methods of Measuring the Source Activity

There are three methods by which the activity of the source was determined. These methods are the change in the mass of the plate, the net flow of charge from the solution to the electroplating substrate, and the radioactivity as measured by a counting experiment. These three methods allowed a consistency check on the amount of ⁵⁷Co measured. A step-by-step procedure of the creation of a radioactive source and the procedure for the three methods of analysis is given in Appendix A. The results for the Mössbauer source are shown in Table 2.

3.3.1 Method 1: Change in Mass

In order to determine the number of ^{57}Co atoms electroplated, a careful record of the change of mass from each step of the procedure was kept. The measurement of the initial mass of the foil was used as a reference to determine the change in mass due to the electroplating process. After the foil was

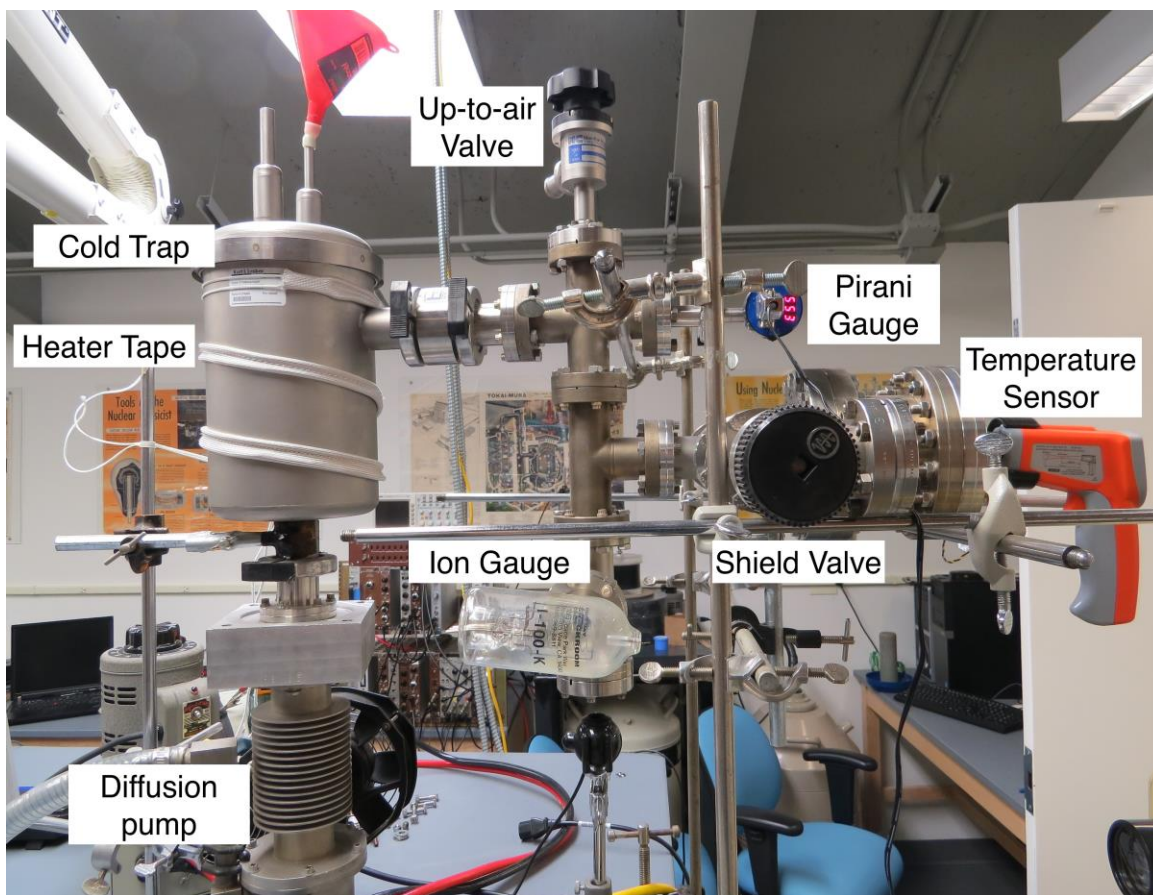


Figure 21. Furnace apparatus. This is a picture of the vacuum chamber used to diffuse the ^{57}Co source into the steel foil. The Pirani gauge measured pressure to the order of mTorr. The diffusion pump was then used to reach lower pressures. The heater tape and cold trap were used to reduce the moisture that is present in the chamber. Once the chamber was evacuated to about 10^{-6} Torr the heating process began. The shield valve was opened and closed to take readings of the temperature of the foil being heated.

cleaned this initial measurement was taken. Once the plate was electroplated, the amount of cobalt electroplated is:

$$\text{Percent Electroplated} = \frac{\Delta m_{\text{foil}}}{m_{\text{Available Co}} \left(\frac{m_{\text{used}}}{m_{\text{total}}} \right)} \quad (3.1)$$

where Δm_{foil} is the change in mass of the foil after and before electroplating. The $m_{\text{Available Co}}$ term is the total mass of the cobalt present in the solution from both ^{57}Co and the ^{59}Co compound. Because the ratio of ^{57}Co to all of the cobalt in solution is present in Δm_{foil} and $m_{\text{Available Co}}$, the ratio cancels. The $m_{\text{used}}/m_{\text{total}}$ term is the percentage of the radioactive solution used out of the total solution made. For a typical case, the values were: $\Delta m_{\text{foil}} = 5.2 \times 10^{-3}$ g, $m_{\text{Available Co}} = m_{^{59}\text{Co}} + m_{^{57}\text{Co}}$, where $m_{^{59}\text{Co}} = 0.0347$ g and $m_{^{57}\text{Co}} = 1.185 \times 10^{-10}$ g, and $m_{\text{used}}/m_{\text{total}} = 0.3963$ g/2.0315 g. The solution drawn out was near 0.5655 ml of 0.5M concentrated electroplating solution. These values from 13 November 2015 electroplated yielded a percent electroplated of 76.81%.

It is necessary in both this method and the electroplated charge method to assume that the ratio of ^{57}Co to ^{59}Co is the same as the ratio of ^{57}Co to ^{59}Co originally introduced to the solution. This assumption was best insured by stirring the radioactive solution containing ^{57}Co right before drawing solution out of the source bottle to electroplate.

3.3.2 Method 2: Electroplated Charge

The electroplating current was also analyzed to determine the total ^{57}Co electroplated to the substrate. The charge of cobalt in the radioactive solution is +2e. By determining the total charge of cobalt that moved within the solution, from the solution to the electroplated foil, the number of atoms of cobalt electroplated to the steel foil was measured by dividing the displaced charge due to the cobalt by +2e. Using the averaged molar mass of the cobalt within the solution then,

$$\text{Percent Electroplated} = \frac{m_{\text{of Co charge}}}{m_{\text{Available Co}} \left(\frac{m_{\text{used}}}{m_{\text{total}}} \right)} \quad (3.2)$$

where $m_{\text{of Co charge}}$ is the calculated value of mass from the charge from integrating the current vs. time plot output from the MS8050 Digital Multimeter as was shown in Figure 20. The denominator is the same as the previous measurement.

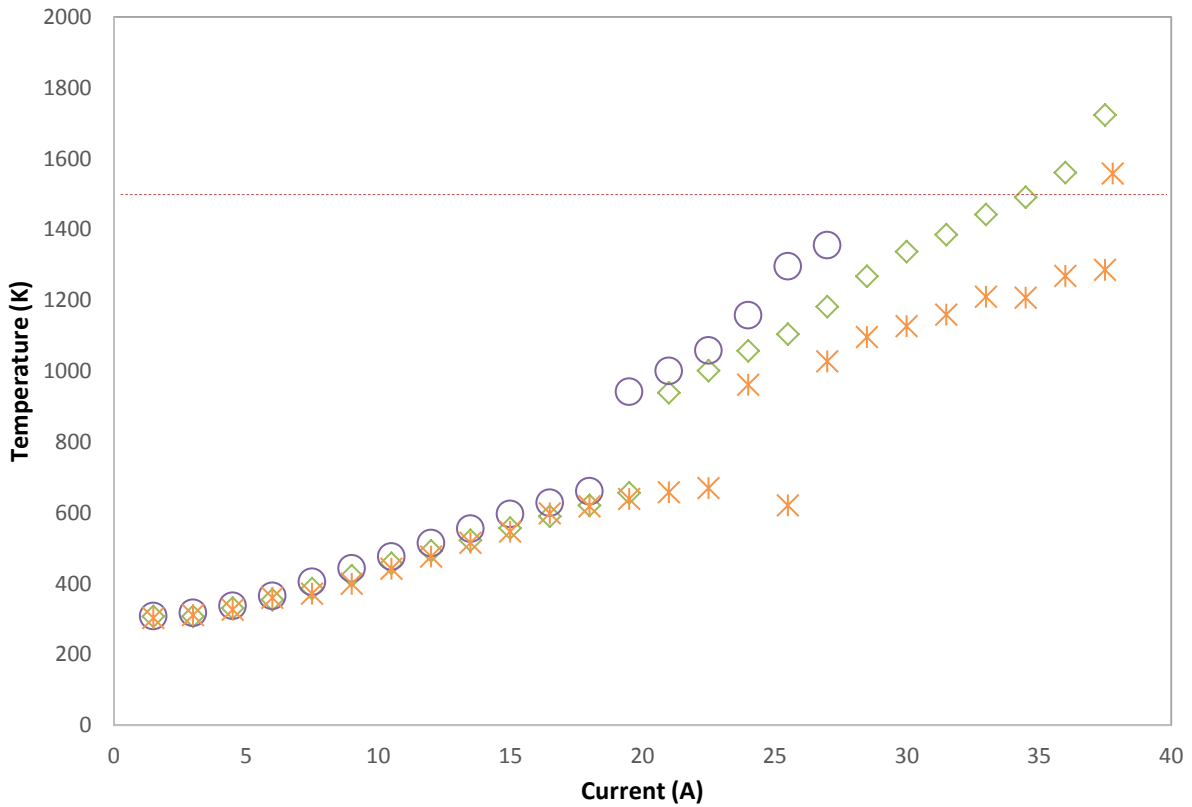


Figure 22. Temperature versus current measurements. The data that are shown are from 30 January 2015 (green diamonds), 6 February 2015 (purple circles), 11 February 2015 (orange crosses). The dotted red line represents the melting point for the 304 stainless steel foil.

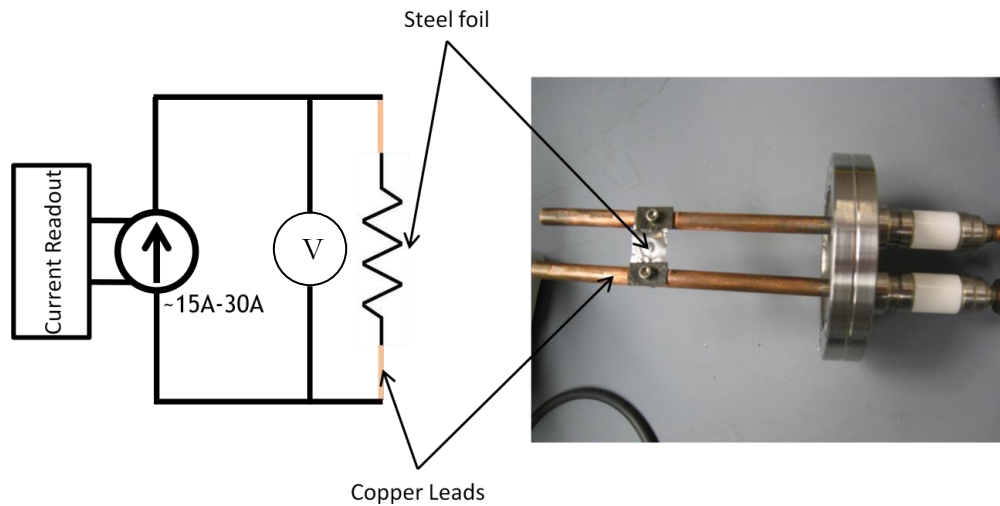


Figure 23. Cobalt diffusion apparatus. The foil heating circuit (left) and the copper rods used in heating (right). The foil was mounted to the copper rods with screws. By placing a potential difference across the leads, a current passed through the foil to heat it. This current was from the Mastech HY1550EX DC Power Supply. The potential difference was measured by a Metex M-4650 Digital Multimeter. This figure was taken from Ref. [20].

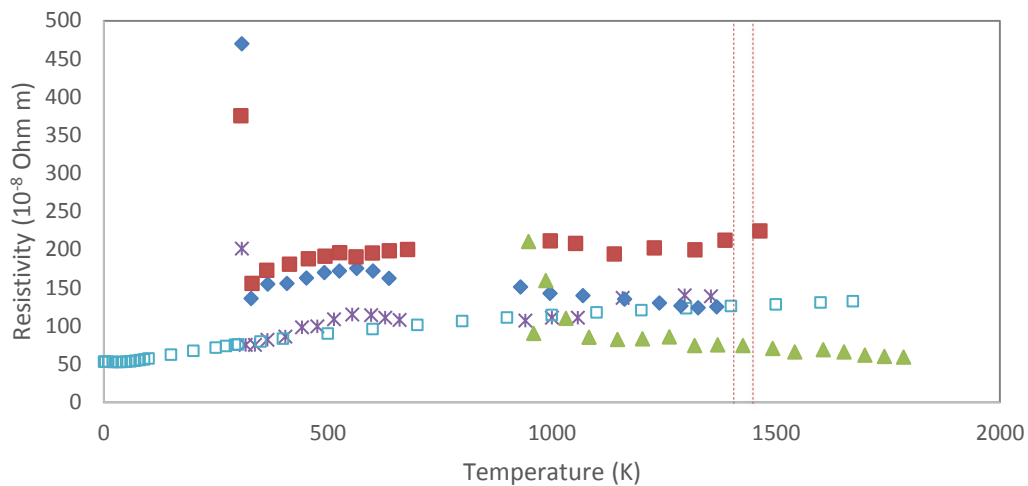


Figure 24. Resistivity measurements. The previously published values (hollow squares) are compared to measurements performed (all other shapes) at Houghton College. The dashed lines are the region in which Type 304 stainless steel melts. The source of disagreement is due to the resistivity of the copper rod used as well as differences in electrical contact between different diffusion processes.

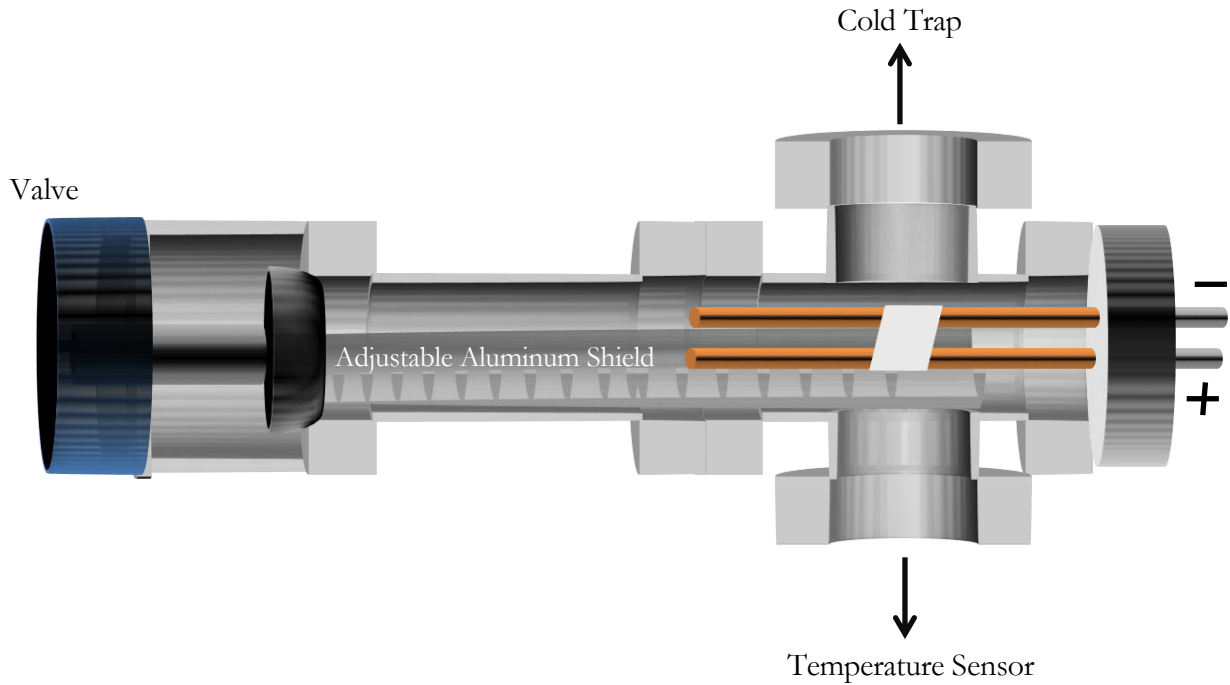


Figure 25. Diagram of the aluminum shield system. This is looking at the rightmost section of the vacuum chamber shown in Figure 21 from above. By adjusting the shield valve the aluminum shield was moved back, allowing the temperature sensor to take a reading. The valve was then closed, moving the aluminum shield back to protect the temperature sensor from any ions sputtered by the foil or copper.

$A \exp(-Ct) + Bt + D$, shown in Figure 20, and integrating the $A \exp(-Ct)$ term over the time, that is,

$$Q_{Co} = \int_0^{t_{run}} A \exp(-Ct) dt \quad (3.3)$$

This value predicted that 1.89 C of charged cobalt ions were electroplated. The $Bt+D$ term is possibly due to the outgas of Cl from solution and the aqueous ions drifting in solution. By dividing the total displaced charge by the charge of ionized cobalt, the number of cobalt atoms was found,

$$N_{\text{Co}} = \frac{18.9 \text{ C}}{2 \times 1.602 \times 10^{-19} \text{ C}} = 5.99 \times 10^{19} \text{ atoms} \quad (3.4)$$

By dividing by Avogadro number the number of moles is found,

$$M_{\text{Co}} = \frac{5.99 \times 10^{19} \text{ atoms}}{6.022 \times 10^{23} \left(\frac{\text{atoms}}{\text{mole}}\right)} = 9.795 \times 10^{-5} \text{ moles Co} \quad (3.5)$$

By multiplying by the ratio of ^{57}Co atoms to all cobalt atoms in solution,

$$M_{^{57}\text{Co}} = 9.795 \times 10^{-5} \text{ moles Co} \times 3.414 \times 10^{-9} \frac{^{57}\text{Co}}{\text{Co}}, \quad (3.6)$$

$$M_{^{57}\text{Co}} = 3.34 \times 10^{-13} \text{ } ^{57}\text{Co moles}. \quad (3.7)$$

By multiplying by the molar mass of ^{57}Co , the $m_{\text{of Co charge}}$ was found

$$m_{\text{of Co charge}} = 3.34 \times 10^{-13} \text{ } ^{57}\text{Co moles} \times 56.94 \frac{\text{g}}{\text{mole}} \quad (3.8)$$

$$m_{\text{of Co charge}} = 1.904 \times 10^{-11} \text{ g} \quad (3.9)$$

This prediction yielded that the percent electroplated was 82.38%.

3.3.3 Method 3: Radioactivity

Using a 1 in. by 2 in. crystal Bicron 2M1/2 Sodium Iodide detector the activity of the source and solution were measured. The NaI detector high voltage was set to 700V and placed 81.4 mm away from the source. A diagram for the counting experiment is given in Figure 26. By recording the radioactivity of the source solution bottle before and after electroplating an idea of how many ^{57}Co nuclei were used from the source bottle was estimated. These spectra were recorded in a Spectech UCS30 MCA. A spectrum of the ^{57}Co source bottle is shown in Figure 27. A background run for this experimental setup is shown in Figure 28. By dividing each channel of the MCA histogram by the time

for the counting run the count rate for each channel was found. The same was done for a background run.

Because the source is radioactive, it was necessary that the timing during the process of creating the source be recorded as well as done rapidly; the production of a source solution, the initial radioactivity measurements, including background and non-radioactive plate spectra, the electroplating of radioactive solution and recording of the source bottle after removal of electroplating solution, the final massing of the electroplate, and radioactivity measurements must be performed consecutively and without long interruption. The longest allowed interruption would be on the order of 2-3 days. That is, since the half life of ^{57}Co is 271.74 days, the interruption of 2-3 days would reduce the activity of the source bottle by 0.5-0.8%. Thus, an assumption that the radioactivity of the source bottle has not changed over the source creation process yields appreciable error rapidly. Thus, in addition to the $\pm 20\%$ error from the manufacturer, an additional error must be considered based on the time elapsed during the experiment.

The energy spectrum of the ^{57}Co electroplated foil was recorded before and after heating the foil to determine how much ^{57}Co was lost during the diffusion process. This was done because it was believed that some cobalt may have evaporated or that the sputtering steel may have carried away cobalt atoms. Energy spectra of the copper rods and the vacuum chamber are shown in Figure 29 and Figure 30. In order to create the histogram for the vacuum chamber, the NaI detector was placed up against the port into which the copper rods were inserted, as is shown in Figure 23. Because of this change in geometry, the background could not be subtracted from this run. It was estimated that 0.5% of the cobalt used was wasted in the diffusion process based on the radioactivity measurements of the electroplated source before diffusion and after diffusion. That is, in addition to the decay of the ^{57}Co atoms in the source, there was an additional loss of 0.5%, which may have been lost in diffusion or due to the change in geometry of the source.

After a spectrum for the diffused ^{57}Co Mössbauer source was taken and the background subtracted out, the remaining ^{57}Co peak that was left was summed by adding the counts of each channel in a cut

placed around the peak to determine the number of counts in the peak. From this value, the number of ^{57}Co nuclei present in the source was determined by dividing the count rate in the peak by the decay constant for ^{57}Co . An absolute full-peak efficiency of 0.0077 was measured using a calibrated ^{68}Ge source, which was then used to measure a radioactivity of about 271 nCi for the ^{57}Co source created.

Table 2. The results of the 13 November 2015 electroplate. The three methods roughly agree on the percentage of solution used that was electroplated. However the predictions of the radioactivity differ greatly. The Radioactive Counting measure was based on the difference in the number of counts of the source bottle before and after electroplating. However, due to the difficulty of determining the efficiencies, a prediction of the error is unknown however it is presumed to be high. The Charge Electroplated and Change in Mass measurements were based on recording the macroscopic quantities of the number of ions drifting in solution and the change in the mass of the solution bottle and foil. The Mettler and Toledo MS 104S/03 Analytical Balances used have very little error in the measurement. Therefore, it is believed that the Change in Mass measure is the most reliable measurement. However, both the Charge Electroplated and Change in Mass measurements are susceptible to predicting lower values, this due to the solution evaporating slowly in between measurements.

Methods	Net % of Used Solution Electroplated	Radioactivity (nCi)
Radioactive Counting	77.52%	271
Charge Electroplated	82.38%	160
Change in Mass	76.81%	149

A counting experiment was performed with the waste solution and electroplating apparatus pieces, including the cathode and glass-T. It was revealed that in the electroplating process the greatest amount of ^{57}Co was lost. These losses were 10-30% of the cobalt used in the solution. This was shown

most readily from radioactivity measurements of the waste solution, the platinum cathode, and the glass-T. The energy spectrum showing the losses in the electroplating process is shown in Figure 31. The counts in the peak were 63240, with a counting time of a few minutes under 2 hours, the rate of counts in the peak was 10.11 counts/sec. The rate found was significant compared to the radioactivity of the electroplate, which was 77.35 counts/sec. These values were raw calculations with no calculated efficiencies due to the difficulty of the geometry.

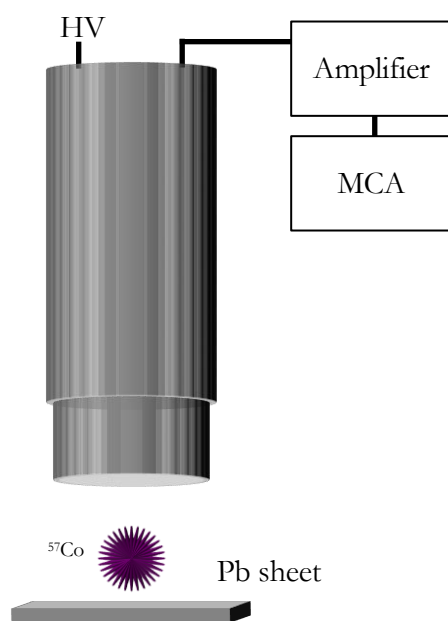


Figure 26. Radioactive counting apparatus. A radioactive ^{57}Co source was placed under a Bicron 2M1/2 NaI detector with cylindrical crystal dimensions of 1 in. by 2 in. height and diameter, respectively. The photomultiplier tube was supplied with 700 V. The whole apparatus was supported by clamps, and the lead sheet was used to support the source beneath the NaI detector. The pulses from the photomultiplier tube were sent into an Ortec Model 485 Amplifier with fine gain of 7 and coarse gain of 4. These pulses were then digitized and made into a histogram by a Spectech UCS30 MCA. The distance from source to detectors was 81.4 mm.

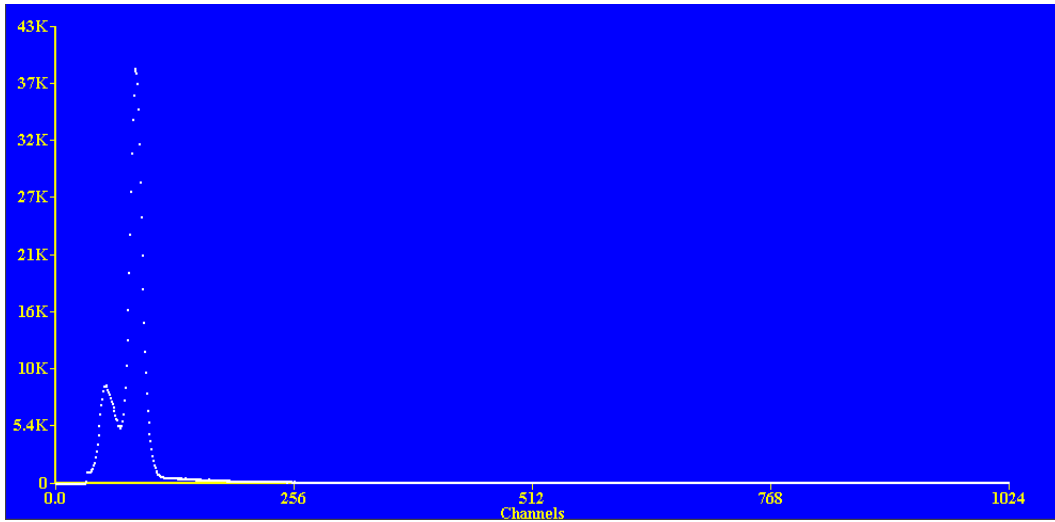


Figure 27. Histogram for the Source bottle of ^{57}Co . The first rise is background and Compton scattering due to the presence of the ^{57}Co source. The second peak is the ^{57}Co 122.1 keV gamma ray. The elapsed time for this run was just under 2 hours. The count rate in the peak, after subtracting background, was 371 counts/sec and the total counts in the peak were 2.2 million.

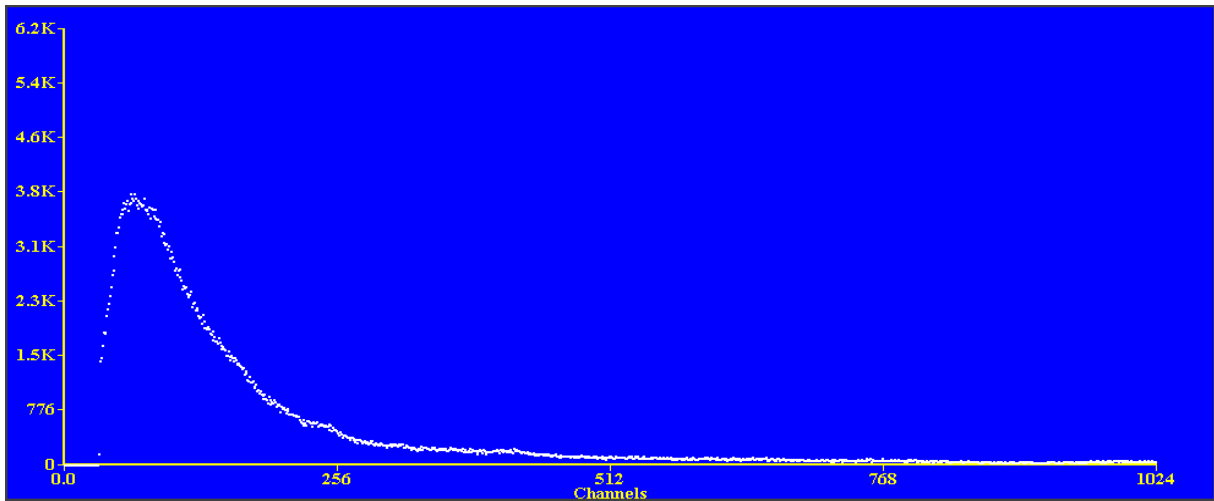


Figure 28. Background radioactivity histogram. This spectrum was taken in order to subtract background from the source bottle and radioactive electroplate spectra. The elapsed time was just over 2 hours.

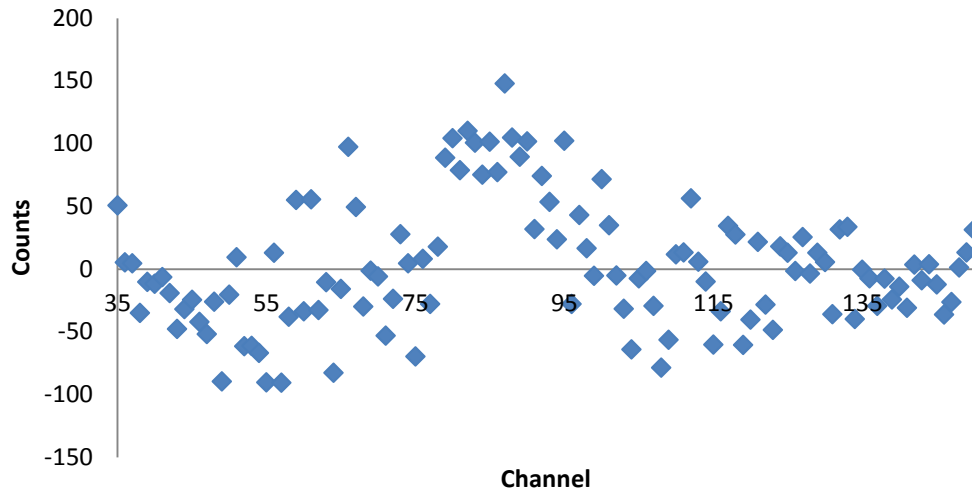


Figure 29. Copper rods radioactivity histogram. An energy spectrum for the copper rods used in the diffusion process with the background subtracted. The number of counts in the peak was roughly 3200, which corresponded to 1.44 counts/sec in the peak.

3.4 Longitudinal Doppler Effect Apparatus

Using the Mössbauer source created by the techniques previously described, the first necessary test is to demonstrate the longitudinal Doppler effect. This is a test of the feasibility of the experimental methods and the Mössbauer source. A diagram is shown in Figure 13 and a photograph of the apparatus is shown in Figure 32.

The experimental apparatus consists of a 120 mm diameter polycarbonate plastic CD of thickness 0.8 mm with a type 304 steel foil of thickness 0.001 in. glued to the face using Bob Smith Industries 5-minute epoxy. The epoxy was the common mixture of a polymercaptan and amine hardener. After this, the disk was fastened onto a Vernier Rotary Motion Sensor. The rotation motion sensor allows the speed of the disk to be monitored and recorded. The gear motor currently being used, an Actobotics gear motor, part number 638142, allows us to achieve a range of the slow velocities on the order of 0.5 RPM at 12 V. A HY3003-3 DC Power Supply was used to supply an adjustable voltage to these gear motors.

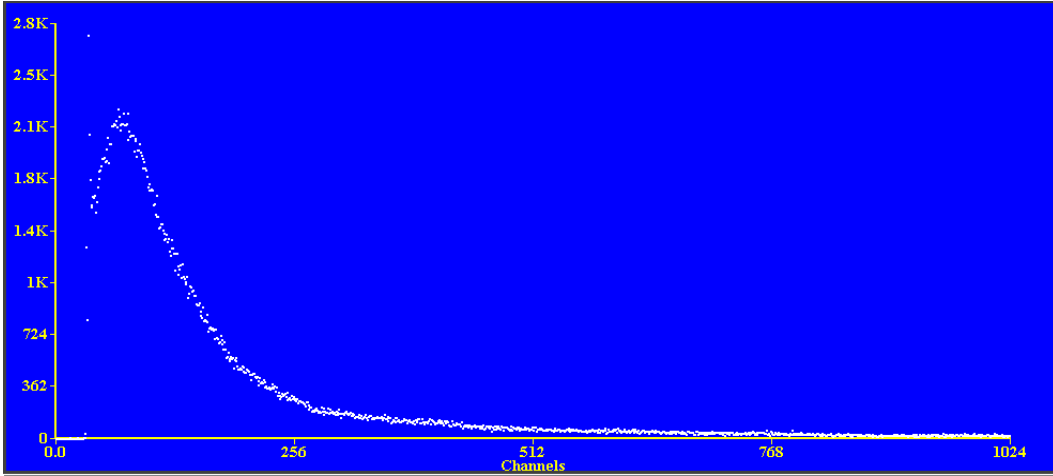


Figure 30. Vacuum chamber radioactivity histogram. There is seemingly no evidence for ^{57}Co in the spectrum, even after a long counting experiment of 6 hours. Comparing to Figure 28, the spectrum looks nearly identical to background.

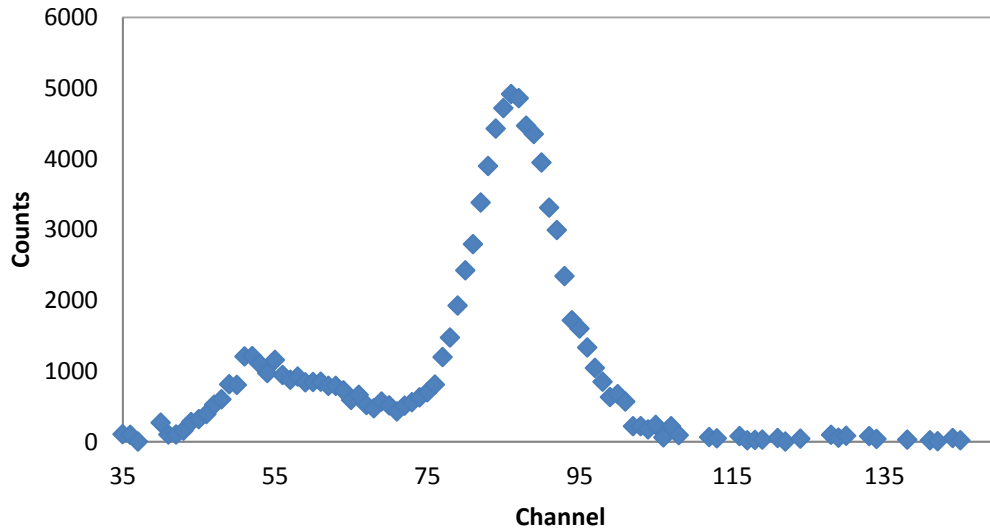


Figure 31. Radioactivity histogram of waste solution. An energy spectrum for the glass-T, waste solution, and electrode with background subtracted. A ^{57}Co peak is visible showing that a significant portion of the ^{57}Co is lost.

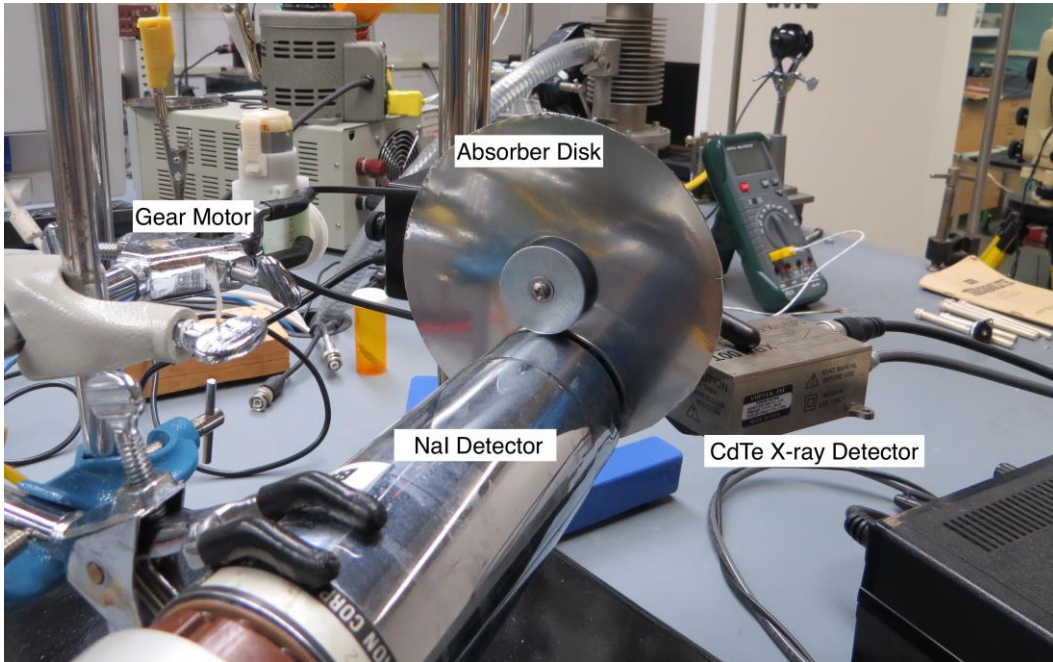


Figure 32. Longitudinal Doppler effect apparatus. The ^{57}Co source, placed on the face of the NaI detector, has the rotating absorber disk between it and the CdTe X-ray Detector. The gear motor is used to spin the absorber disk. The rotary motion sensor state is read out to a computer allowing for the speed of the absorber to be calculated.

By rotating the absorber at different constant rotational velocities and using NIM electronics recorded a Spectech UCS30 MCA the experiment is able to sweep through the absorption spectrum. The NIM circuit is shown in Figure 33. Unlike previous experiments, Houghton College intends to use a coincidence system to demonstrate the longitudinal Doppler and subsequently the transverse Doppler effect. The pulses from the NaI detector are amplified by an Ortec Model 485 Amplifier and then discriminated by an Ortec Model 551 Timing Single Channel Analyzer (TSCA) that produces logic pulses for only the 122.1 keV gamma rays. The TSCA worked such that if an analog pulse passed into the TSCA is of a voltage that the pulse is contained within the discriminator voltage levels, the TSCA will release a logic pulse. These discriminator levels were determined by using a Spectech UCS30 MCA and the timing by a Tekronix TDS2024 Oscilloscope. The logic pulses from the TSCA, signaling the detection of a 122.1 keV gamma ray from the NaI detector, started the clock on the Ortec 467 Time-to-amplitude-Converter (TAC). A few tens of nanoseconds after the 122.1 keV gamma ray, the 14.4 keV gamma ray will be emitted and can be detected by the Amptek XR-100T-CdTe X-ray detector. If

detected, then the pulse will be amplified in an Ortec 485 Amplifier. The 14.4 keV amplified pulse is then discriminated by an Ortec Model 455 TSCA. The TSCA logic pulses are split and sent to the TAC stop input and then an Ortec Model 416A Gate & Delay Generator in order to delay the amplified 14.4 keV pulse to allow processing time at the TAC. This pulse is then sent to the input of an Ortec Model 426 Linear Gate. Meanwhile, the TAC processes the timing difference between the 122.1 keV and 14.4 keV gamma rays. The TAC output is discriminated by the TSCA selecting output voltages corresponding to the width of the timing spectrum peak. The output of this TSCA is used as the gate logic pulse for the Linear Gate, which allows only the X-ray detector spectrum in coincidence with the 122.1 keV gamma ray to be recorded into the Spectech UCS30 MCA.

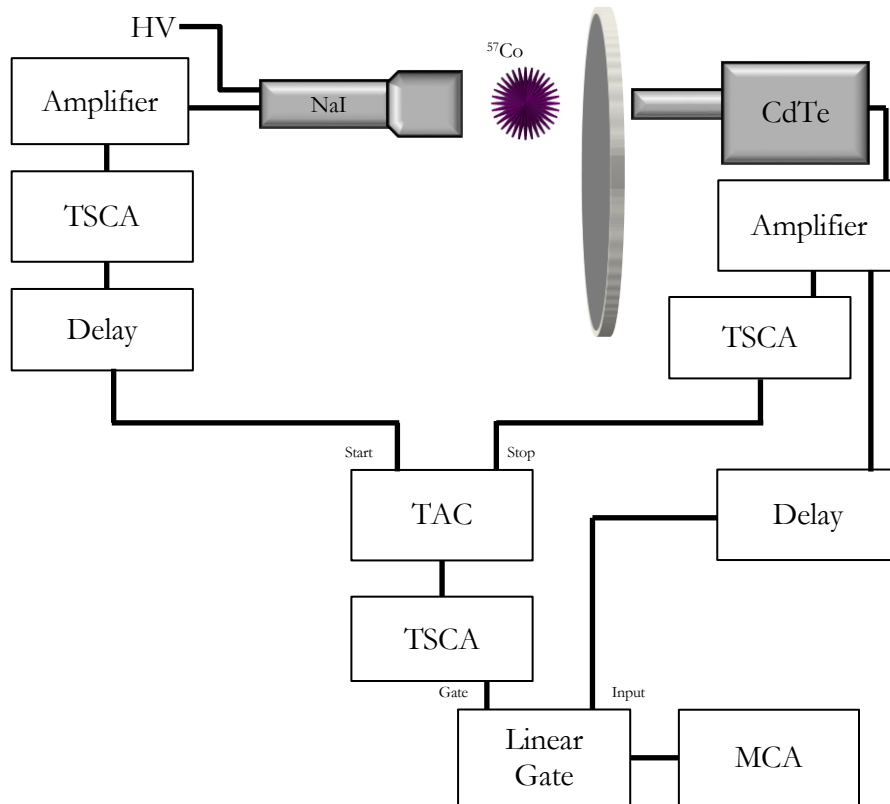


Figure 33. Longitudinal Doppler effect circuit diagram. The ^{57}Co cascade of 122.1 keV to 14.4 keV allows the use of coincidence methods to produce a spectrum for the X-rays emitted simultaneously with the 122.1 keV gamma ray.

Chapter 4

CONCLUSION AND FUTURE PLANS

In the early 1960s the Mössbauer effect was used to demonstrate general relativity using both the transverse Doppler effect and the gravitational redshift. The Mössbauer effect allows for very precise measurements of frequency shifts as small as one part in 10^{15} . Historically, the sources used in these previous experiments tended to be 1mCi or higher. However, at Houghton College, the use of low activity sources is desirable, so a procedure for creating low activity Mössbauer sources using ^{57}Co has been worked out. By using three different calculation methods, the radioactivity of the source was determined. Substantial progress has been made towards demonstrating the longitudinal Doppler effect with this source, including constructing the experimental apparatus and initial tests of gear motors to produce the rotational speeds desired. After demonstrating the longitudinal Doppler effect, it is the next goal of Houghton College to demonstrate general relativity using the transverse Doppler effect. This will require that a relatively stronger, 1-10 μCi , source be used as well as a motor to achieve speeds of 20,000 RPM, as shown in Eq. 2.33. To achieve such speeds it is believed that we may be able to use a CD drive motor. Because the speed of the disk may approach the breaking apart limit for the absorber used, a safety system surrounding the spinning disk will be necessary. All of these challenges, and likely many more to reveal themselves, will need to be overcome in order to demonstrate general relativity.

Appendix

EXPERIMENTAL PROCEDURE

Step 1: Beginning to clean a foil:

- 1.1 Put on rubber gloves.
- 1.2 Rinse your rubber gloves with distilled (DI) water and then with Isopropanol.
- 1.3 Locate the Type 302 Steel Foil.
- 1.4 Cut a 13.5 mm by 26 mm piece. It is critical that the 13.5 mm measurement is exact.
- 1.5 Puncture the furnace mounting holes before beginning the cleaning process.
- 1.6 Once you have acquired a good foil, rinse the foil with DI.
- 1.7 Rinse the foil with Isopropanol.
- 1.8 Rinse the foil with DI.

Step 2: Removing Inorganic Materials:

- 2.1 Wear safety goggles.
- 2.2 Bring the following items to a chemistry fume hood:
 - The cleaned foil,
 - Two 2 glass beakers (25 mL),
 - A pair of metal tongs
 - The radioactive source bottle (new or old),
 - The cobaltous chloride hexahydrate ($^{59}\text{CoCl}_2 \cdot 6\text{H}_2\text{O}$) compound,

The HCl 0.1M and 12M,

Kim-wipes,

and a log book with a pen.

2.3 Now, pour 10 mL of 12 M HCl into one of the beakers and dilute with 10 mL of DI water.

2.4 Take the metal tongs and the cleaned foil and dip the steel foil 2/3 of the total length of the foil into the 12 M HCl and DI.

2.5 Keep the foil inside of the 12 M HCl and DI solution until bubbles begin to form. At this point Fe-Cl bonds are precipitating in the solution. Stir the solution with the foil slightly, then remove the foil.

2.6 Rinse the foil with DI.

2.7 Switch which length the tongs hold on to and repeat the previous 3 substeps.

2.8 After rinsing the foil with DI again, gently dry the foil with kim wipes, being sure not to create bends in the foil.

2.9 Place the foil into the second beaker.

2.10 Place this beaker in a desiccator or desiccating oven.

2.11 Dispose of the 12M HCl and DI solution.

2.12 Wash the beaker.

2.13 Wash the metal tongs thoroughly with DI.

Step 3: Creating the Radioactive solution:

3.1 Locate an analytical balance.

3.2 Take the new source bottle and remove the protective tape.

- 3.3 Mass the radioactive source bottle without the tape.
- 3.4 With the cleaned first beaker it is desired to make a 0.5M solution.
- 3.5 Measure out a value near 1.8021 g of 0.1 M HCl.
- 3.6 Transfer the HCl into the radioactive source bottle.
- 3.7 Mass the new source bottle with HCl.
- 3.8 Acquire a plastic tray.
- 3.9 Zero the analytical balance with the plastic try on the balance.
- 3.10 Place a value near 0.1353 g of $^{59}\text{CoCl}_2\cdot 6\text{H}_2\text{O}$ on the plastic tray.
- 3.11 Place the measured $^{59}\text{CoCl}_2\cdot 6\text{H}_2\text{O}$ into the new source bottle.
- 3.12 Mass the source bottle with the $\text{HCl} + ^{59}\text{CoCl}_2\cdot 6\text{H}_2\text{O}$.
- 3.13 Carefully remove the beaker containing the steel foil from the desiccator.
- 3.14 Mass the steel foil.

Step 4: Radioactivity:

- 4.1 Take the radioactive source bottle and place it in your counting apparatus.
- 4.2 Check the pulses on an Oscilloscope from the phototube to an MCA.
- 4.3 Dimensions need to be taken, due to their vital nature to the counting geometry and will be used to help calculate efficiencies.
- 4.4 The MCA Spectrum, depending on the specifics of the experimental apparatus and geometry being used, it will look like Figure 27.
- 4.5 Wait until good counting statistics are achieved, 10,000 counts minimally in peak.
- 4.6 This higher number of counts is necessary later for determining the cuts on the peak.

4.7 Perform a background count; placing the clean foil in the counting apparatus and waiting a time equivalent to that for the source bottle spectra.

Step 5: Electroplating:

5.1 Once the source bottle and the background radioactivity measurements have been taken, take the foil and fasten the glass-T atop it.

5.2 Fill the glass-T to the shoulder with the radioactive solution.

5.3 Place the cathode in the glass-T.

5.4 Tie the positive lead from the HY3003-3 DC Power Supply to the platinum cathode.

5.5 Tie the negative lead from the HY3003-3 DC Power Supply to the foil.

5.6 Set the voltage to 3.75 V.

5.7 Adjust the distance of the electrode to the plate to be 10 mm.

5.8 While this is electroplating one can acquire a radioactivity reading for the now reduced source bottle activity, being sure to separate the electroplating apparatus from the counting apparatus to avoid the possibility of picking up the ^{57}Co source being electroplated in the spectrum.

Step 6: Diffusion:

6.1 After finishing the electroplating process and the reduced source bottle counting run, take the waste solution, glass-T, and cathode placing them into the counting apparatus for a time similar to that of the background run.

6.2 Store the reduced ^{57}Co source solution with the other sources.

6.3 Fastened the foil inside of the furnace.

- 6.4 Sealing the vacuum chamber, turn on the fore-pump, checking beforehand that the oil level on the fore-pump is sufficient.
- 6.5 Once the pressure reaches the order of a mTorr, turn on the diffusion pump, with its cooling fan.
- 6.6 After 2-3 hours, turn on the ion gauge to determine the pressure.
- 6.7 If the pressure is at 10^{-5} Torr, turn on the heater tape for a half hour.
- 6.8 Once the half hour is up turn off the heater tap.
- 6.9 Acquire about a quart of liquid nitrogen.
- 6.10 Pour the liquid nitrogen into the cold trap.
- 6.11 Watch the pressure gauge for it to reach 10^{-6} Torr or lower.
- 6.12 Once 10^{-6} Torr has been reach, and before connecting the leads of the power supply to the copper rods, turn the Coarse Current and Voltage O.V. of the HY1550EX DC Power Supply to the maximum before turning the power supply on.
- 6.13 Turn the power supply on.
- 6.14 Turn the Coarse Current all the way down.
- 6.15 Turn the Fine Voltage all the way up.
- 6.16 Turn the Coarse Voltage up about a quarter revolution of the dial.
- 6.17 Turn the Coarse Current up slightly and set it to 1.5 A, the power supply is now a current source.
- 6.18 Set the emissivity of the temperature sensor to 0.25-0.30, the published values for type 304 stainless steel are in this range.
- 6.19 In the following order record the data:

The pressure from the Ion Gauge Controller,

The voltage between the two leads connecting the foil inside the vacuum chamber,

The temperature of the foil through the Temperature sensor, doing this last allowed the foil to respond to the change in current. Using the shield valve, open the valve and take a reading and then immediately begin closing the shield valve. Remembering to keep the valve slightly open to prevent the volume inside the valve to continue to be evacuated.

6.20 Iterate this process until the foil reaches 1000 °C.

6.21 Bake the foil for 2 hours, monitoring the temperature of the foil every 5 minutes.

6.22 Turn the HY1550EX DC Power Supply off, letting the system settle.

6.23 Wait a few moments until the foil cools to 100°C before turning off the diffusion pump, then bringing the vacuum chamber up to air, followed finally by turning the fore-pump off.

6.24 A radioactivity measurement of the foil is to be taken.

6.25 A Mössbauer source has been created.

References

- [1] J. Rayleigh, *Scientific Papers* (Univ. Press, Cambridge, 1912), Pg. 7-26.
- [2] R. Wood and J. H. Moore, *Astrophysical J.* **18**, 94 (1903).
- [3] H. Frauenfelder, *The Mössbauer Effect* (W.A. Benjamin, New York, 1962), Pg. 1-2.
- [4] W. Lamb, *Phys. Rev.* **55**, 190 (1939).
- [5] R. Mössbauer, presented at The Nobel Prize Award Ceremony and Nobel Banquet, Stockholm, Sweden, (1961).
- [6] A. Bearden, *Am. J. Phys.* **32**, 109 (1964).
- [7] H. Frauenfelder, *The Mössbauer Effect* (W. A. Benjamin, New York, 1962), Pg, 101-126.
- [8] R. Pound and G. Rebka, *Phys. Rev. Lett.* **3**, 439 (1959).
- [9] R. Pound and G. Rebka, *Phys. Rev. Lett.* **3**, 554 (1959).
- [10] R. Pound and G. Rebka, *Phys. Rev. Lett.* **4**, 337 (1960).
- [11] R. Pound and G. Rebka, *Phys. Rev. Lett.* **4**, 274 (1960).
- [12] W. Kündig, *Phys. Rev.* **129**, 2371 (1963).
- [13] H. Hay, J. P. Schiffer, T. E. Cranshaw, and P.A. Egelstaff, *Phys. Rev. Lett.* **4**, 165 (1964).
- [14] A. Kholmetskii, M. Mashlan, B. Rogozev, K. Ruebenbauer and D. Zak, *NIM B* **108**, 359 (1996).
- [15] A. Kholmetskii, T. Yarman, and O. Missevitch, *Phys. Scr.* **77**, 1 (2008).
- [16] A. Kholmetskii, T. Yarman, O. Missevitch and B. Rogozev, arXiv 0812.4507, 2008 (unpublished).
- [17] Spectrum Techniques, 106 Union Valley Rd, Oak Ridge, TN 37830
- [18] M. R. Bhat, *Nuclear Data Sheets* **85**, 415 (1998).
- [19] E. Preikschat, Ph.D. thesis, University of Birmingham, 1968.
- [20] K. Mann, B.S thesis, Houghton College, 2013.